AD NUMBER

ADB001019

NEW LIMITATION CHANGE

TO

Approved for public release, distribution unlimited

FROM

Distribution authorized to U.S. Gov't. agencies only; Test and Evaluation; AUG 1974. Other requests shall be referred to Commander, Edgewood Arsenal, ATTN: SAREA-TS-R, Aberdeen Proving Ground, MD 21010.

AUTHORITY

D/A EA ltr dtd 17 Jun 1975

EDGEWOOD ARSENAL CONTRACT REPORT
ED-CR-74021

OPTICAL TECHNIQUES FOR THE REMOTE DETECTION OF BIOLOGICAL AEROSOLS

Final Comprehensive Report

By:

John Oblanas
David Ross
Vincent Simmon
F. L. Ludwig
Michael Anbar

August 1974

STANFORD RESEARCH INSTITUTE
MENLO PARK, CALIFORNIA 94025

DEPARTMENT OF THE ARMY
Headquarters, Edgewood Arsenal
Aberdeen Proving Ground, Maryland 21010

DISCLAIMER

The findings in this report are not to be construed as an official Department of the Army position unless so designated by other authorized documents.

DISPOSITION

Destroy this report when no longer needed. Do not return it to the originator.

SECURITY CLASSIFICATION OF THIS PAGE (When Data Entered)

REPORT DOCUMENTATION PAGE

READ INSTRUCTIONS BEFORE COMPLETING FORM

1 REPORT NUMBER: ED-CR-74021

2. GOVT ACCESSION NO.:

3 RECIPIENT'S CATALOG NUMBER:

4. TITLE (and Subtitle): OPTICAL TECHNIQUES FOR THE REMOTE DETECTION OF BIOLOGICAL AEROSOLS

5. TYPE OF REPORT & PERIOD COVERED: Final Report

6. PERFORMING ORG. REPORT NUMBER: SRI Project 2046

7. AUTHOR(s): John Oblanas, David Ross, Vincent Simmon, F. L. Ludwig, and Michael Anbar

8. CONTRACT OR GRANT NUMBER(s): Cont. DAAA15-72-C-0338

9. PERFORMING ORGANIZATION NAME AND ADDRESS: Electronics and Radio Sciences Division, Stanford Research Institute, Menlo Park, California 94025

10. PROGRAM ELEMENT, PROJECT, TASK AREA & WORK UNIT NUMBERS:

11. CONTROLLING OFFICE NAME AND ADDRESS: Commander, Edgewood Arsenal, Attention: SAREA-TS-R, Aberdeen Proving Ground, Maryland 21010

12 REPORT DATE: August 1974

13. NO. OF PAGES: 109

15. SECURITY CLASS. (of this report): UNCLASSIFIED

14. MONITORING AGENCY NAME & ADDRESS (if diff. from Controlling Office): Commander, Edgewood Arsenal, Attention: SAREA-DE-DB, Aberdeen Proving Ground, Maryland 21010 — Frank Wagner, Project Officer 671-4110

15a. DECLASSIFICATION/DOWNGRADING SCHEDULE: NA

16. DISTRIBUTION STATEMENT (of this report)

Distribution limited to U.S. Government agencies only because of test and evaluation of commercial products. Other requests for this document must be referred to Commander, Edgewood Arsenal, Attn: SAREA-TS-R, Aberdeen Proving Ground, Maryland 21010.

JAN 1975

17. DISTRIBUTION STATEMENT (of the abstract entered in Block 20, if different from report)

18. SUPPLEMENTARY NOTES

19. KEY WORDS (Continue on reverse side if necessary and identify by block number)

Pathogenic organisms
Fluorescence
Excitation spectra
Aerosol
Lidar
Remote detection

20. ABSTRACT (Continue on reverse side if necessary and identify by block number)

Laboratory and remote detection experiments with optical techniques demonstrated the feasibility of remote fluorescence detection of biological aerosols. Laboratory measurements of fluorescence response of five types of bacteria were best characterized by excitation spectra. A lidar field experiment verified the principle of fluorescence detection of biological aerosols under atmospheric conditions and enabled evaluation of achievable remote sensing performance. Performance calculations indicated that an optical detection of 14 cells per

DD FORM 1 JAN 73 1473
EDITION OF 1 NOV 65 IS OBSOLETE

SECURITY CLASSIFICATION OF THIS PAGE (When Data Entered)

19. KEY WORDS (Continued)

20 ABSTRACT (Continued)

liter of air could be achieved at a range of 2 kilometers at sea level in mid-latitude locations. Recommendations are given for further research.

SUMMARY

The overall purpose of the research reported in this document was to conduct exploratory development studies to determine the suitability and reliability of utilizing the radiative response of microbiological material in aerosol form, induced by a laser light source, for remote detection and quantification of the presence of microbiological materials in the ambient atmosphere with minimum response time. The net result of these studies establishes the initial feasibility of developing concepts and equipment for the remote detection of these aerosols.

This research effort was conducted in two separate phases:

(1) Laboratory experiments

(2) Remote detection experiments.

In the first phase, the optical characteristics of several selected biological materials were measured to obtain spectral signature and intensity data. These data were used to estimate the performance characteristics of a hypothetical remote optical sensor. Results indicated that the detection range of 1-2 kilometers (km) could ultimately be achieved.

The second phase of this work consisted of a series of simple remote detection experiments to:

- Verify the theoretical calculations.
- Demonstrate the feasibility of the concept.
- Obtain a reliable estimate of sensor performance based on measured parameters.

The results of these experiments confirmed the earlier calculations.

The conclusions derived from this research are as follows:

(1) The basic principle of remote fluorescence detection of biological aerosols has been demonstrated under ambient atmospheric conditions.

(2) Based on experimental data, the sensitivity of a state-of-the-art optical remote sensor, specifically designed for this application, is estimated to be in the order of 14 cells per liter of ambient air at a range of 2 km at sea-level, midlatitude geographical locations.

PREFACE

The work described in this report was authorized under Contract DAAA 15-72-C-0388, Project 2046 dated 29 June 1972, between Edgewood Arsenal and Stanford Research Institute. The research work was started in July 1972 and completed in December 1973.

The use of trade names in this report does not constitute an official endorsement or approval of the use of such commercial hardware or software. This report may not be cited for purposes of advertisement.

ACKNOWLEDGMENTS

The authors gratefully acknowledge the technical advice and assistance provided by Mr. Frank Wagner and Mr. Harry DeLong of Edgewood Arsenal.

CONTENTS

SUMMARY 3

PREFACE 4

ACKNOWLEDGMENTS 4

LIST OF ILLUSTRATIONS 7

LIST OF TABLES 9

I INTRODUCTION 11

II METHOD OF APPROACH 15

A. Objective 15

B. Rationale 15

III PHASE I--LABORATORY EXPERIMENTS 19

A. Introduction 19

B. Experimental Apparatus 19

1. Fluorometer 19
2. Pulsed Fluorometer 23
3. Nebulizer 26

C. Experimental Techniques 27

D. Results 28

1. Media 28
2. Bulk Liquid Suspensions of Organisms 29
3. Polarization Experiments 40
4. Fluorescent Lifetime Measurements 40
5. Bacterial Aerosols 47
6. Quantum Yield Measurements 49
7. Preliminary Calculations of Range Performances . . 51
8. Aerosol Diffusion Model 54
9. Discussion and Summary of Results--Phase I 61

IV PHASE II--REMOTE DETECTION EXPERIMENTS 67
A. Introduction 67
B. Experimental Apparatus 67
C. Aerosol Column 69
D. Remote Sensing Apparatus 72
E. Experimental Procedure 75
F. Results 78
G. Discussion and Summary of Results--Phase II 96
V CONCLUSIONS 101
VI RECOMMENDATIONS 105
LITERATURE CITED 109

ILLUSTRATIONS

1	Block diagram of modified spectrofluorometer	21
2	Block diagram of Optitron pulsed fluorometer	25
3a	Washed Escherichia coli in isotonic saline solution	33
3b	E. coli metabolic products	33
4a	E. coli irradiated for 15 minutes with a 10-sun Xenon lamp	34
4b	E. coli heated to 100°C for 7 minutes	34
5a	Pseudomonas aeruginosa in isotonic saline solution, exposed to 10-sun Xenon lamp for 15 minutes	35
5b	P. aeruginosa metabolic products	35
6	Bacillus subtilis washed and suspended in isotonic saline solution	36
7	Staphylococcus aureus washed and suspended in isotonic saline solution	37
8	Streptococcus faecium washed and suspended in isotonic saline solution	38
9	Typical examples of pulsed fluorometer data	44
10	Pulsed fluorometer output versus time	45
11	Excitation of E. coli aerosol with distilled water aerosol as reference, followed at 350 nm	48
12	Excitation of P. aeruginosa aerosol with distilled water aerosol as reference, followed at 475 nm	49
13	Relative spectral intensity of illumination incident on fluorometer sample cell (uncorrected for detector response).	50
14	Relative spectral response of fluorometer detector to 3000°K black body source	51
15	Mass concentrations (μgm m^{-3}) for line release--Case 1	61
16	Mass concentrations (μgm m^{-3}) for line release--Case 2	62
17	Size distributions at different locations in the cloud--Case 2	63

18 Configuration for the remote sensing experiments 68

19 The SRI Mark IX lidar system 70

20 Aerosol column 71

21 Typical examples of remote fluorescence data: fluorescein aerosol 79

22 Typical examples of remote fluorescence data: P. aeruginosa aerosol--first experiment 83

23 Typical examples of remote fluorescence data: P. aeruginosa aerosol--second experiment 89

TABLES

1	Characteristics of the Modified Spectrofluorometer	20
2	Fluorescence Data for Several Media	29
3	Fluorescence Data for Several Bacteria	31
4	Parameters Used in Modeling Concentrations from an Instantaneous Line Source	60
5	Modified Mark IX Lidar Characteristics	74
6	Modified Mark IX Lidar--Optical Losses	98

OPTICAL TECHNIQUES FOR THE REMOTE DETECTION OF BIOLOGICAL AEROSOLS

I INTRODUCTION

This report describes the research conducted during the first phase of an exploratory investigation into the feasibility of utilizing certain optical interactions for remote sensing of biological aerosols. The research was carried out by a team of specialists drawn from three divisions of SRI, namely, Physical Sciences, Life Sciences, and Electronic and Radio Sciences. The investigation was conducted during the period July 1972 to December 1973, under the auspices of the Department of the Army, Edgewood Arsenal, Maryland (Contract No. DAAA 15-72-C-0338).

The objective of an effective remote detection and warning system for the presence of viable pathogens in the atmosphere is to distinguish reliably between dangerous concentrations of viable biological and other particulate aerosols. Since some pathogenic organisms undergo deactivation when exposed to air and sunlight, it is also important to distinguish between aerosols of viable organisms and deactivated ones.

The two methods to determine the age of an aerosol are to monitor either physical or chemical changes. The physical approach involves monitoring changes of gross characteristics of the aerosol with time, such as changes in cloud shape, concentration, or particle size distribution. These characteristics can, in principle, be monitored remotely by optical methods; however, sole reliance on physical characteristics may result in ambiguities.

The chemical approach involves monitoring chemical changes brought about in the biological aerosol by exposure to light and oxygen. These

chemical changes in turn produce changes in the optical characteristics of the aerosol, and thus are measurable.

Any practical optical method has to be evaluated according to a number of criteria:

(1) It must be sensitive enough to detect a potentially dangerous aerosol in the presence of ambient background.

(2) It must distinguish between biological and nonbiological aerosols, by detection and quantitative assay of characteristic constituents.

(3) It preferably should distinguish between a viable fresh pathogen and an aged harmless one.

(4) It must have a short response time, so as to allow rapid scanning and early warning.

(5) It must be mobile, rugged, easy to handle, and reasonably priced.

In the course of laser-related research during the past decade, a number of optical techniques have been identified which could, in theory, provide the specificity and sensitivity required for this application. Continuing developments in laser research have greatly increased the number of laser wavelengths available, and have achieved dramatic increases in laser energy levels. These improvements in laser technology could permit practical utilization of various optical techniques which in the past have been limited by practical considerations.

Optical techniques potentially applicable to remote sensing applications include: fluorescent and phosphorescence, Raman scattering, resonant enhancement of Raman or fluorescent signals, and multiwavelength differential absorption.

As will be evident from the discussions in subsequent sections of this report, there is little specific information available to evaluate properly the feasibility of the various possible classes of remote

detection systems, particularly in the area of optical characteristics of specific microorganisms, and their associated media. The one detailed effort we are aware of, a study by IBM on the fluorescence characteristics of some aerosolized biological materials, provided some positive indication of the feasibility of this approach to the problem of remote detection.[1]*

Our research was primarily concerned with obtaining experimental measurements of the optical characteristics of a small group of carefully selected bacteria, and using this limited data base to form a preliminary assessment of feasibility. The information in this report represents the results of an initial investigation into several technical areas where the required information was either unavailable or, if available, was not in a form ready for analysis. Because of this limited scope, the report cannot discuss all possible considerations inherent in remote optical detection technology, but concentrates on the significant, first-order considerations of feasibility of a practical detection system.

---

*References are listed at end of report.

II METHOD OF APPROACH

A. Objective

The objective of this research was to conduct exploratory studies of the optical properties of certain aerosols to establish the feasibility of developing methods and equipment for the remote detection of aerosols, using optical techniques.

B. Rationale

SRI Proposal ERU 72-62, which led to this project, describes several optical interactions that potentially could be applied to remote sensing. These interactions are: Raman scattering, fluorescence and phosphorescence, resonant enhancement of Raman or fluorescent signals, and multiwavelength differential absorption.

The optical interactions were reviewed early in the project, with particular emphasis on their advantages and limitations within the specific context of remote detection. Fluorescent techniques appear to offer likelihood of success in a short time period, because the fluorescent signature is relatively intense (compared with that of Raman scattering), and it is specific and characteristic of biological systems. Other properties of the fluorescent signature, such as its polarization and lifetime, offer additional possibilities for improved background discrimination and identification. Also, a remote sensor based on fluorescence techniques could be a relatively simple device, from both hardware and signal processing considerations. It is possible, however, that Mie backscattering from the aerosol at the incident wavelength may

be useful for range determination of the time of absorption to which the time of fluorescence is referred. If feasible, differential absorption techniques may be used in conjunction with fluorescence measurements to obtain additional information on the aerosol. We believe, however, that the information provided by the fluorescence measurement would not require supplemental information on the absorption spectrum of the aerosol.

Raman scattering does not appear particularly promising for this application, because of its relatively small scattering cross section, and because the Raman scattering signature could be obscured by the relatively intense fluorescence associated with the aerosol.[2,3*] This fluorescence background might be suppressed to some degree by wavelength selection, time discrimination, or resonant enhancement techniques. However, because Raman measures rotational-vibrational excitations, the spectrum obtained from a complex target such as an aerosol will itself be extremely complex and not amenable to diagnosis.

Theoretically, resonant enhancement techniques (resonant fluorescence or resonant Raman scattering) could result in increased scattering cross sections, thereby increasing detection range performance. Resonant effects are being investigated in connection with air pollution applications. Preliminary results indicate that these resonant effects may be more applicable to Raman scattering than to fluorescence techniques. It should be noted that biological aerosols, unlike the simple diatomic and triatomic air pollutants investigated, exhibit band absorption

---

*Also, J. Oblanas, Addendum to Final Report, "The Application of Lidar Probing Techniques for the Remote Detection of Aerosals," SRI Project 7971, Contract N00140-69-C-0429 with the U.S. Naval Weapons Laboratory (March 1971).

rather than line absorption and are thus much less likely to gain sensitivity from resonance techniques. The possibility of exploiting resonance effects to enhance fluorescent cross sections should be investigated after the preliminary feasibility of the basic fluorescence technique has been established.

In view of these considerations, we have concentrated our efforts on the potential use of fluorescence techniques. Our approach consisted of two relatively independent research phases. In the first phase laboratory experiments were carried out with a small number of selected microorganisms, both in suspension and in aerosol form. A calibrated analytic fluorometer was used to obtain the excitation and fluorescent spectra, the amplitudes of which were related to previously established calibration standards. The purpose of these laboratory experiments was to establish that microorganisms in aerosol form have characteristic excitation and fluorescent spectra and to obtain data regarding the efficiency of this process. These data were then used to obtain preliminary estimates of the theoretical performance of a state-of-the-art optical sensor system.

The estimates were favorable, and a second research phase was initiated. Remote detection experiments were conducted to demonstrate the feasibility of the concept under simulated field conditions, and to obtain experimental data on which more reliable estimates of system performance could be based.

III PHASE I--LABORATORY EXPERIMENTS

A. Introduction

A detailed discussion of the laboratory measurements phase of the research program is presented in this section, including such t pics as experimental apparatus, laboratory methods, data and results obtained, and analysis.

The laboratory measurements of the optical parameters of aerosols were performed using a modified spectrofluorometer, an ultrasonic aerosol generator, and an aerosol flow system which conducted the aerosol to a flow-through sample cell located in the fluorometer. This apparatus was used to obtain the excitation and emission spectra of selected microorganisms, both in suspension and in aerosol form. In addition, brief, exploratory investigations were conducted into the polarization properties and the excitation lifetime characteristics of selected materials to determine the usefulness of these independent parameters to the problem under consideration.

The data obtained were subsequently analyzed, and the results were used as a basis upon which the theoretical performance of a state-of-the-art optical sensor could be estimated.

B. Experimental Apparatus

1. Fluorometer

An SRI-owned Baird-Atomic spectrofluorometer (Model SF-1) was selected for the laboratory measurement program because its sample compartment is compatible with the straight-through aerosol flow system

(to be described later), and because of its relatively high sensitivity, and excellent rejection of scattered light. In Table 1 are listed the pertinent characteristics of this instrument. The electronics associated with the SF-1 were found unsuitable for the specific requirements of the planned measurement program because of a high internal noise level, general insensitivity, and unacceptably large drifts in the calibration or the system. Accordingly, the original electronics of the SF-1 were extensively modified, using equipment available at SRI. A block diagram of the modified fluorometer is shown in Figure 1.

TABLE 1: CHARACTERISTICS OF THE MODIFIED SPECTROFLUOROMETER
(Baird-Atomic Model SF-1)

Excitation source:	D.C. xenon arc - 150 watts
Monochromators:	Double-pass, dual-plane relfection gratings (600 lines per millimeter)
Wavelength range:	2200 angstrom units (Å) - 7000 Å
Wavelength resolution:*	320 Å, 80 Å, 20 Å (full bandwidth, half power)
Sensitivity:	1 PPB quinine sulphate in 0.1 N sulphuric acid with 10:1 signal-to-noise ratio
Detector:	RCA 1P28 9-stage photomultiplier (S-5 cathode) operated at 1108 volts (V) (10^6 gain)
Dynamic range:	5 decades of light intensity in 11 selectable linear amplitude ranges
Accuracy of intensity measurements:	± 3% of full-scale reading of selected intensity range
Calibration standard:	Raman spectrum of distilled water
Scan speed:	26 Å per second

*All measurements presented in this report were at a spectral resolution of 80 Å for both excitation and fluorescence monochromators.

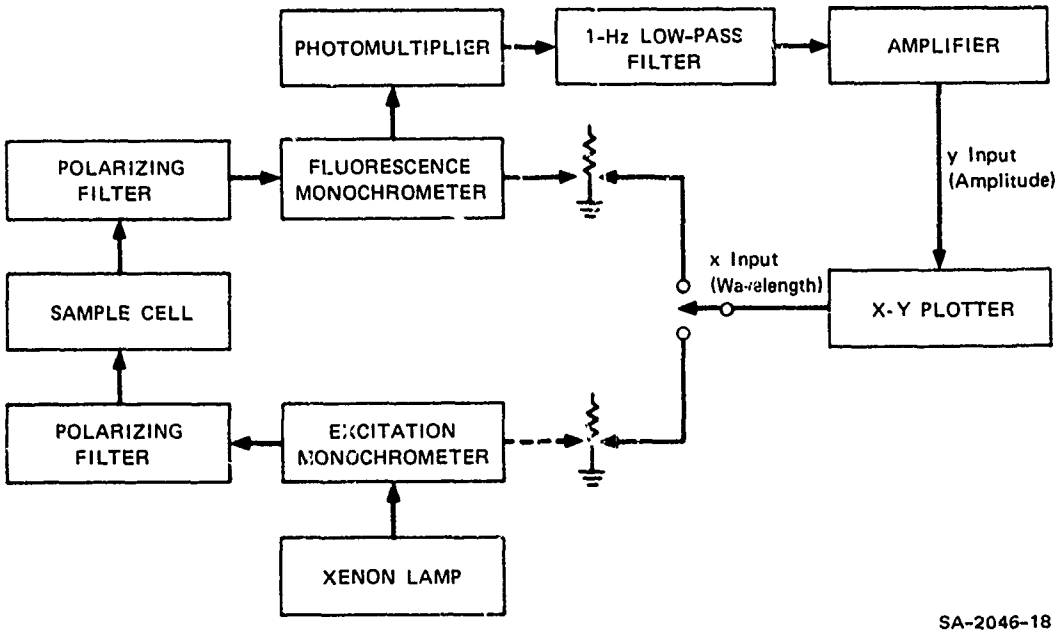

Figure 1 Block diagram of modified spectrofluorometer

The original optical detector in the SF-1 was replaced with a 1P28 photomultiplier (quartz window, S-5 photocathode), selected for high quantum efficiency and high internal gain. The original photomultiplier high-voltage power supply, which exhibited very poor regulation characteristics, was replaced with a well-regulated power supply whose output voltage could be accurately varied.

The signal-to-noise ratio of the new photomultiplier was experimentally optimized by varying the photomultiplier anode voltage to maximize the ratio of the Raman scattering band of distilled water to the background noise level of the photomultiplier. This setting of the high-voltage power supply (1108 volts) was used for all subsequent experimental measurements.

The anode current output of the photomultiplier was filtered by a 1-Hertz (Hz) low-pass filter. This reduced the noise level inherent in the signal by increasing the integration time to the maximum allowed

by the response time of the X-Y plotter. The signal was then amplified by a selectable gain current-to-voltage conversion amplifier. The output voltage was applied to the X-axis of an X-Y plotter. The same output voltage was also displayed on a calibrated meter, which thus directly monitored the output current of the photomultiplier. An indication of the photomultiplier output current was required to avoid possible measurement errors, resulting from photomultiplier saturation at high light intensities.

These modifications allow the accurate measurement and comparison of fluorescent emission over a dynamic range of five decades of light intensity, with a recording capability extending over 11 selectable linear amplitude ranges. Each range can be recorded to an accuracy of ± 3% of full-scale reading for that range.

The excitation and emission monochromator wavelength drives were positioned in the conventional way; that is, either drive can be positioned manually or driven by a synchronous motor at a scan rate of 2.6 nanometers per second (nm/sec). The X axis of the X-Y plotter was driven in the usual way by a dc voltage, proportional to the wavelength setting of either the excitation or fluorescence monochromator, generated by two linear potentiometers connected to the output shafts of the excitation and fluorescence monochromator drives.

It was originally planned to monitor the xenon arc lamp intensity by means of a solid-state detector, which was to be added to the fluorometer lamphouse. The output current of this detector could be read on a separate microammeter, allowing independent monitoring of lamp performance and aging. This step was found to be unnecessary, however, because of the absence of any significant short-term fluctuations in the xenon lamp output intensity. The long-term decrease in lamp intensity, from aging, was monitored by the method described below.

A procedure was devised to monitor any degradation in fluorometer performance, or change in its calibration. On a regularly scheduled basis during the measurement program, the following parameters were measured:

(1) Photomultiplier dark current.

(2) Stray light levels within the sample compartment at six discrete wavelength settings of the fluorescence monochromator.

(3) Raman spectra of a reference sample of distilled water to verify both excitation and fluorescence monochromator wavelength calibration; to evaluate the signal-to-noise ratio of the photomultiplier; and to monitor any drift in xenon arc lamp output intensity, arc position, or photomultiplier sensitivity.

(4) Scattered light intensity (using the same reference sample of distilled water). This measurement was made at six discrete wavelengths with both excitation and fluorescence monochromators set at identical wavelengths. This allowed the monitoring, on a relative basis, of the long-term degradation of the xenon arc lamp, particularly at the ultraviolet (UV) end of the spectrum.

Since Tests (3) and (4) monitor the relative performance of lamp and photomultiplier combined, the exact cause of any appreciable deviation from normal performance could be isolated by removing the photomultiplier and independently checking its spectral sensitivity, using standard optical calibration equipment.

No significant changes have been noted in fluorometer performance, except for a slow degradation of xenon lamp intensity with time.

2. Pulsed Fluorometer

We investigated the possibility of converting the existing SF-1 fluorometer to also measure fluorescent lifetimes using the single pulse method. A pulsed arc source was mounted in place of the existing

continuous arc lamp to determine the magnitude of the optical transmission losses in the fluorometer. These were found to be too great to make this approach practical with the available light source. An estimated two orders of magnitude improvement in the fluorometer sensitivity would be required to detect the fluorescence emission of strongly fluorescent materials. While this improvement might be achieved by making major modifications in the existing machine (for example, by converting the existing double-pass monochromators into single-pass monochromators, and by replacing the 1P28 photomultiplier with one of higher gain and quantum efficiency), changes of this magnitude were felt to be unwarranted in the context of a feasibility experiment; accordingly, other approaches were investigated.

About this time SRI learned that Optitron, Inc., Torrance, California, had completed a prototype of a pulsed fluorometer, using a pulsed arc source of less than 1 nanosecond (nsec) decay time, and consisting of a modular assembly of the various optical elements. Unlike most conventional fluorometers, these elements can be rearranged to allow operation either as a filter fluorometer, as a single monochromator, or as a double monochromator fluorometer. A block diagram of the Optitron fluorometer used in the measurements described below is shown in Figure 2.

The arc source emits pulses of 60 watts peak power of 1 nsec and 0.5 nsec decay time, at a repetition rate of 1 kilohertz (kHz). A single-pass grating monochromator, 30-nanometer (nm) spectral interval, was used to define the excitation wavelength. A Corning 7-54 filter provided additional blockage of excitation energy at wavelengths greater than 390 nm. The samples were contained in a conventional Suprasill quartz sample cell, $1 \times 1 \times 4$ centimeters (cm).

A low-pass filter was used to pass the fluorescence emission to the photomultiplier and to block the excitation energy. A 1P28

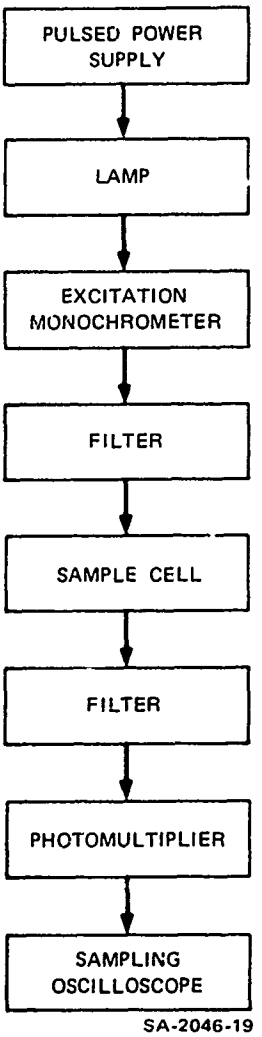

Figure 2 Block diagram of Optitron pulsed fluorometer

photomultiplier, operated at an anode voltage of 850 V, with a conventional voltage distribution on the dynodes, was used as a detector. The photomultiplier output current was displayed as a function of time on a Tektronix 564 oscilloscope with a 3S76 sampling plug-in.

The experimental data obtained with this apparatus are presented in Section D-4.

3. Nebulizer

With the ultrasonic nebulizer, it is possible to obtain a stable, narrow drop size distribution in the low micrometer size range, and to maintain a high concentration. A DeVilbiss Model 35 ultrasonic nubulizer was used to produce the aerosols used in these experiments. This device employs a lead zirconate titanate transducer operating in the longitudinal mode at a frequency of 1.35×10^6 Hz. According to the manufacturer's specifications, the device produces a water-base aerosol with a mass median diameter of approximately 5 micrometers (μm). The nebulization rate at maximum setting is 3 ml/minute.

The manufacturer's estimate of mass median diameter was checked by microphotographic means. In this experiment, a distilled water aerosol was illuminated by a pulsed xenon light source of 1-mic econd (μsec) duration and photographed by conventional techniques. Typical magnifications of 100:1 were used. Because of the illumination geometry used, the aerosol droplets within the depth-of-field of the camera were recorded as bright, sharp semicircles of light. Particles outside the effective depth-of-field were recorded as blurred circles. The scale of the images was established by photographing a conventional stage micrometer placed within the depth-of-field of the camera.

Based on analysis of 4:1 enlargements of these images (not suitably reproducible here) it was established that approximately 95%, by weight, of the aerosol lies in the 2-7 μm diameter range, with a mass median diameter of approximately 5 μm.*

*Personal communication, C. E. Lapple, SRI.

The above measurements represent a first attempt at the relatively difficult task of in-situ measurement of the dynamic characteristics of aerosols. Much more effort could be expended to further refine this and other measurement techniques. However, it was felt that the experimental data obtained so far were adequate to confirm the manufacturer's estimate of mass median diameter and that additional effort at this time was unwarranted in the light of higher priority tasks in this project.

C. Experimental Techniques

The bulk liquid experiments were performed in 1-cm diameter quartz cylindrical cuvettes. Although in these experiments the organism suspensions were decidedly milky and, in some cases, translucent, no optical difficulties were encountered.

Five different bacteria were studied: Pseudomonas aeruginosa, Escherichia coli, Staphylococcus aureus, Streptococcus faecium, and vegetative Bacillus subtilis. (In this report these will be abbreviated as follows: P. aeruginosa, E. coli, S. aureus, S. faecium, and B. subtilis.)

These organisms were chosen for the initial survey since they were reasonably different in their fluorescence characteristics, and the samples were conveniently prepared and handled. These bacteria were suspended in either isotonic saline or glucose minimal medium. Neither medium is fluorescent, and the suspension densities were on the order of 10^7 organisms/cc. Generally, the organisms studied had been centrifuged from the appropriate nutrient medium and resuspended in either isotonic saline or glucose minimal medium two to three hours before optical study. However, in the cases of E. coli and B. subtilis, both washed and unwashed vegetative samples were examined to allow distinction between the organisms and their metabolic products.

The aerosol measurements were performed with an instrumental arrangement in which a quartz tube, leading up from a DeVilbiss Model 35 ultrasonic nebulizer, was passed through the sample compartment of the spectrofluorometer and then to a dry ice acetone-cooled trap. The nebulizer reservoir was loaded with about 10 ml of the above suspensions. Although the trap effectively contained the aerosol, a glass wool plug was affixed to the trap exit stem to ensure against leakage into the laboratory.

The aerosol generator was fed by dry air from a compressed gas cyclinder with a two-stage pressure regulator flowmeter, and a needle-valve flow controller. There was little effect of flow rate on the aerosol spectra, and in work reported the flow rate was set at 450 ml/min.

The five microorganisms used in this project were prepared using the following procedure: A 500-ml flask containing 100 ml of trypticase soy broth media was inoculated with a microorganism and grown at 37°C on a shaker overnight. The overnight cultures were washed three times by centrifugation at 7500 × g for 10 minutes and resuspended in an equal volume of saline solution. After the final centrifugation, the cells were resuspended in one half volume of saline solution. Four hours after the cells were washed, they were submitted to fluorometry.

D. Results

1. Media

It was of interest to distinguish between the organism spectra, and spectra of typical nutrient media used in sample preparation. In Table 2 the fluorescence data for four common media are presented and, as can be seen, the materials display generally similar characteristics.

TABLE 2: FLUORESCENCE DATA FOR SEVERAL MEDIA

Medium	Fluorescence max. (nm)	Excitation max. (nm)	Amplitude (μA)
Brain heart infusion broth	470	398	1.4
Trypticase soy broth	472	403	1.8
Nutrient broth	448	380	2.5
Sabouraud dextrose broth	439	375	1.0

2. Bulk Liquid Suspensions of Organisms

Suspensions of microorganisms in nonfluorescent media were studied initially to provide preliminary data for the subsequent aerosol work. The literature[4] describes the results of some fluorescence studies on a small number of organisms; however, only the fluorescent spectra of the bacteria were reported.*

In our initial measurements we found the fluorescent spectra of the organisms to be characteristically broad, featureless bands of little diagnostic use. Consequently, this approach was not continued. The excitation spectra, on the other hand, were considerably sharper, and in some cases showed detailed structure. As illustrated below, our efforts, therefore, were restricted to the excitation spectra.

---

*The term fluorescent spectrum applies to a spectrum obtained with the excitation monochromator fixed at a given wavelength and the analytical monochromator slowly scanning over a wide energy range. An excitation spectrum is obtained with the alternate arrangement, in which the excitation monochromator scans while the analytical monochromator is fixed.

The data for the organisms are shown in Table 3. In contrast to the spectra for the nutrient media, the fluorescent characteristics of the organisms are rather complex, and show qualitative differences.

The peak (excitation, 300 nm; fluorescence, 350 nm), attributed to tryptophan,[4] appeared in all organism spectra shown in Table 3, but in none of the medium spectra. This peak appears to be a distinguishing feature of bacterial organisms, and since tryptophan is present in the media at concentrations comparable to those prevailing in the microorganisms, it suggests that tryptophan incorporated in native proteins has a much more intense fluorescence. (Considerably more concentrated suspensions could be prepared, and, in principle, the weaker bands could be studied in detail. Concentration quenching does not apply to these systems, where the "local" concentration of an optical center is independent of the microorganism concentration.)

The excitation spectra obtained for the organisms, as well as, for some cases, changes in spectra brought about by lethal heat and sun irradiation treatments are displayed in Figures 3 through 8. We felt it important to measure the spectra of organisms subjected to these lethal treatments, since material encountered under true field conditions could reasonably be expected to contain greater or lesser numbers of organisms killed by sunlight or heat.

The number alongside a band indicates the fluorescence monochromator setting for that band. Figures 3a and 3b present the excitation spectra of E. coli and its metabolic products. The fluorescence of the latter has maxima at wavelengths 447 and 525 nm, different from the 348- and 417-nm peaks of the organism. The 348-nm fluorescent excitation is the ubiguitous tryptophan peak. The double 417-nm peak seems to be characteristic of E. coli. After E. coli were exposed for 15 minutes to a xenon lamp sunlight simulator (10 × sunlight intensity), the excitation spectra at 348 and 417 nm changed significantly, as

TABLE 3: FLUORESCENCE DATA FOR SEVERAL BACTERIA

Organism		Fluorescence Monochromator Setting[a] (nm)	Excitation (nm)	Amplitude (μA)[b]
Gram-negative	Pseudomonas aeruginosa	348[c]	300	0.57
	Metabolic products[e]	473	400	22
	Escherichia coli	348[c]	300	0.92
		417	300, 345[d]	0.13
	Metabolic products[e]	447	365	1.2
		525	f	0.4-0.5
Gram-positive	Staphylococcus aureus	361[c]	310	0.25
		403	345	1.2
		496	340[g]	0.34
	Streptococcus faecium	348[c]	303	1.0
		413	330	0.96
		513	340[g]	0.27
	Bacillus subtilis (vegetative)	353[c]	305	0.91
		405	340	1.3
		509	345[g]	0.26
	Metabolic products[e]	455	h	0.80

Footnotes on following page

Footnotes to table 3

[a]The fluorescence monochromator in each case is set at a maximum signal response for the given excitation wavelength.

[b]Values correspond to the amplitude of the band maximum. The signal levels will, of course, vary with the concentration of the organisms in the suspension. The suspensions dealt with here are on the order of 10^7 organisms/cc, a level that is convenient to work with. The signal levels noted are those for specific cultures. Given the vagaries of culture preparation and instrument sensitivity, the absolute signal level for any band for a given culture could vary by factors of two to three. The relative amplitudes for several bands in a specific culture, however, should be constant to about 30%.

[c]Tryptophan peak.

[d]A pair of peaks of about equal amplitude. The band at 300 nm is probably the tryptophan peak.

[e]Determined through a study of the supernate of the centrifuged organisms.

[f]A complex band in the range 380 to 470 nm.

[g]The spectrum at this fluorescence setting peaks at 340 nm and shows some fine structure from 400 to 478 nm. This fine structure appears to be diagnostic for each gram-positive organism.

[h]A broad, flat-topped band between 325 and 375 nm.

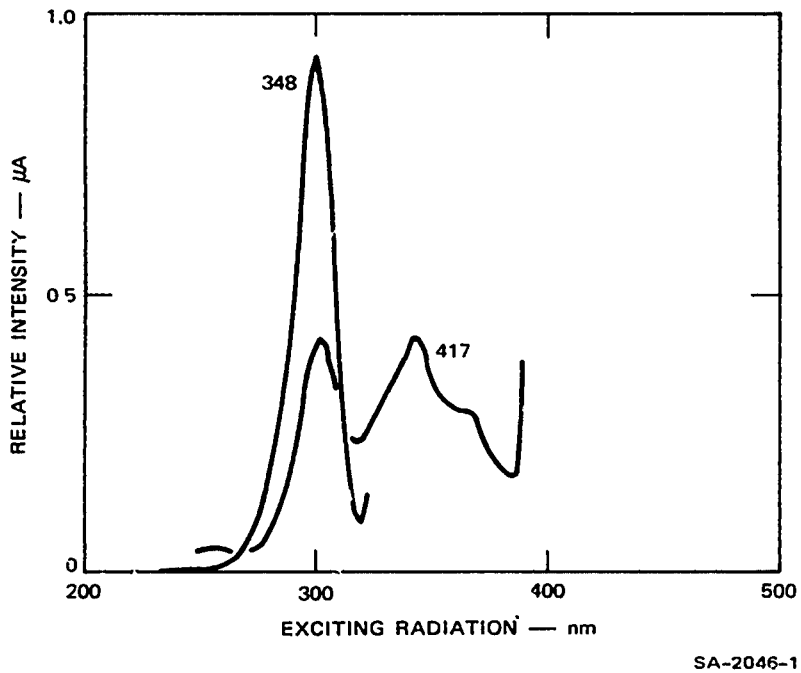

Figure 3a Washed Escherichia coli in isotonic saline solution

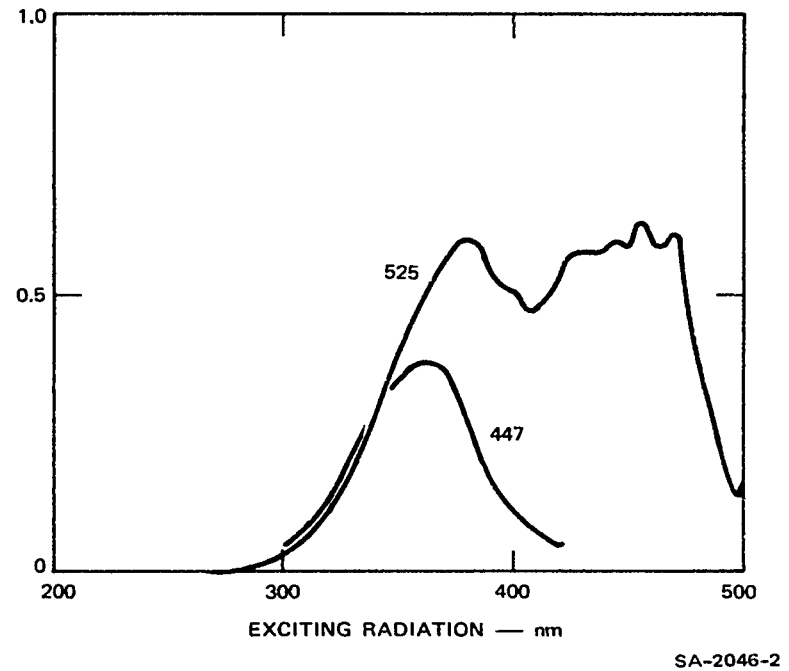

Figure 3b E. coli metabolic products

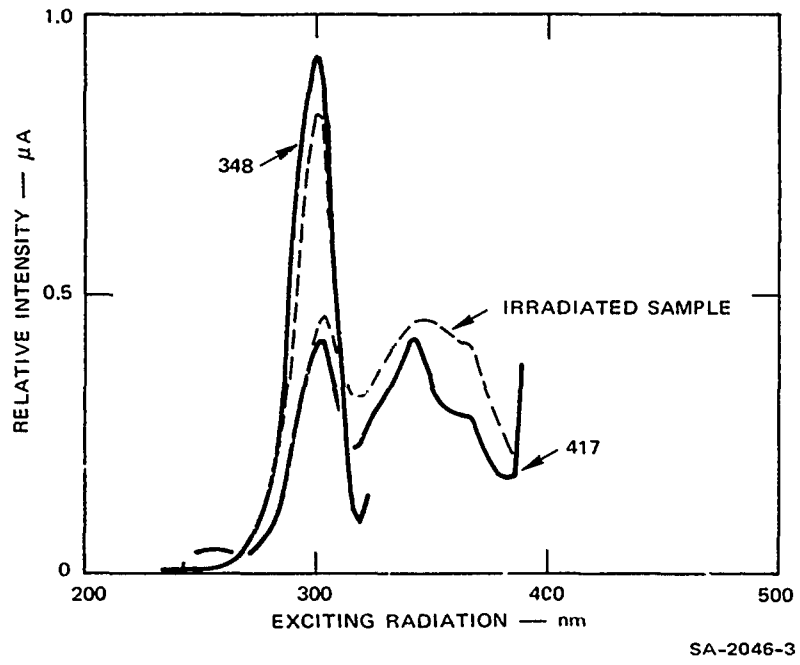

Figure 4a E. coli irradiated for 15 minutes with a 10-sun Xenon lamp 99% mortality.

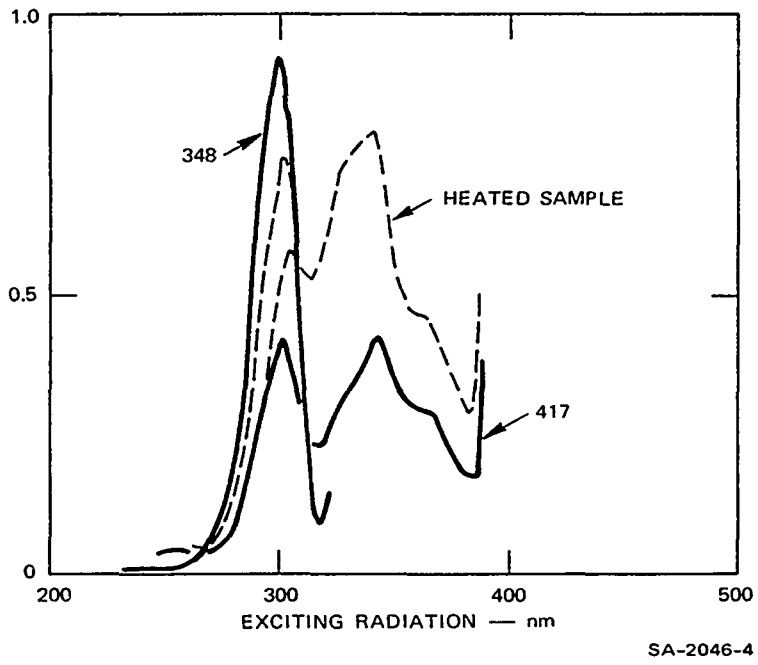

Figure 4b E. coli heated to 100°C for 7 minutes 100% mortality.

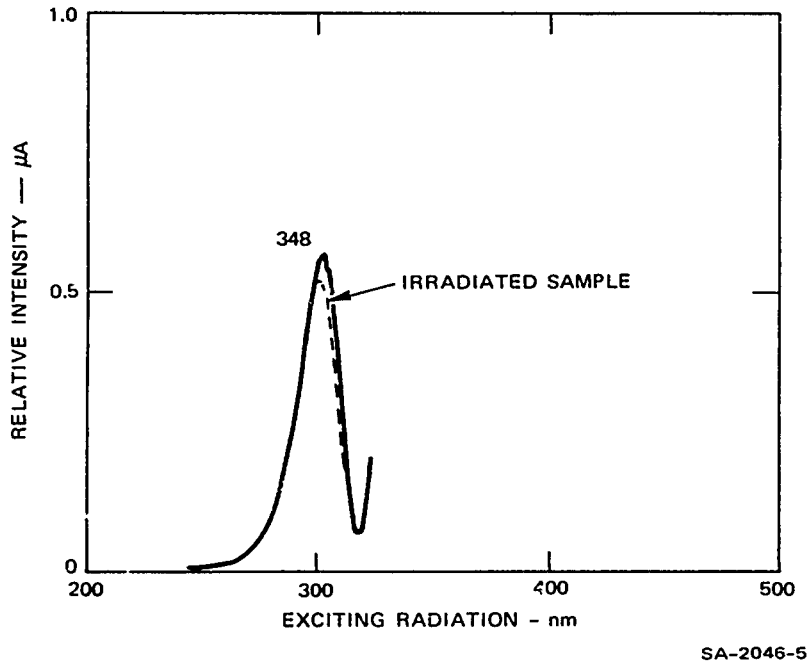

Figure 5a Pseudomonas aeruginosa in isotonic saline solution, exposed to 10-sun Xenon lamp for 15 minutes 99% mortality.

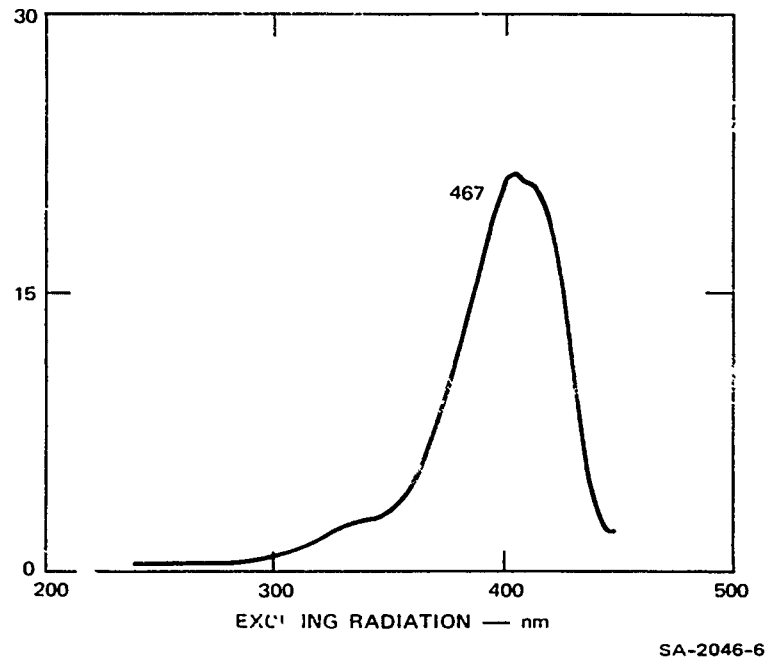

Figure 5b P. aeruginosa metabolic products

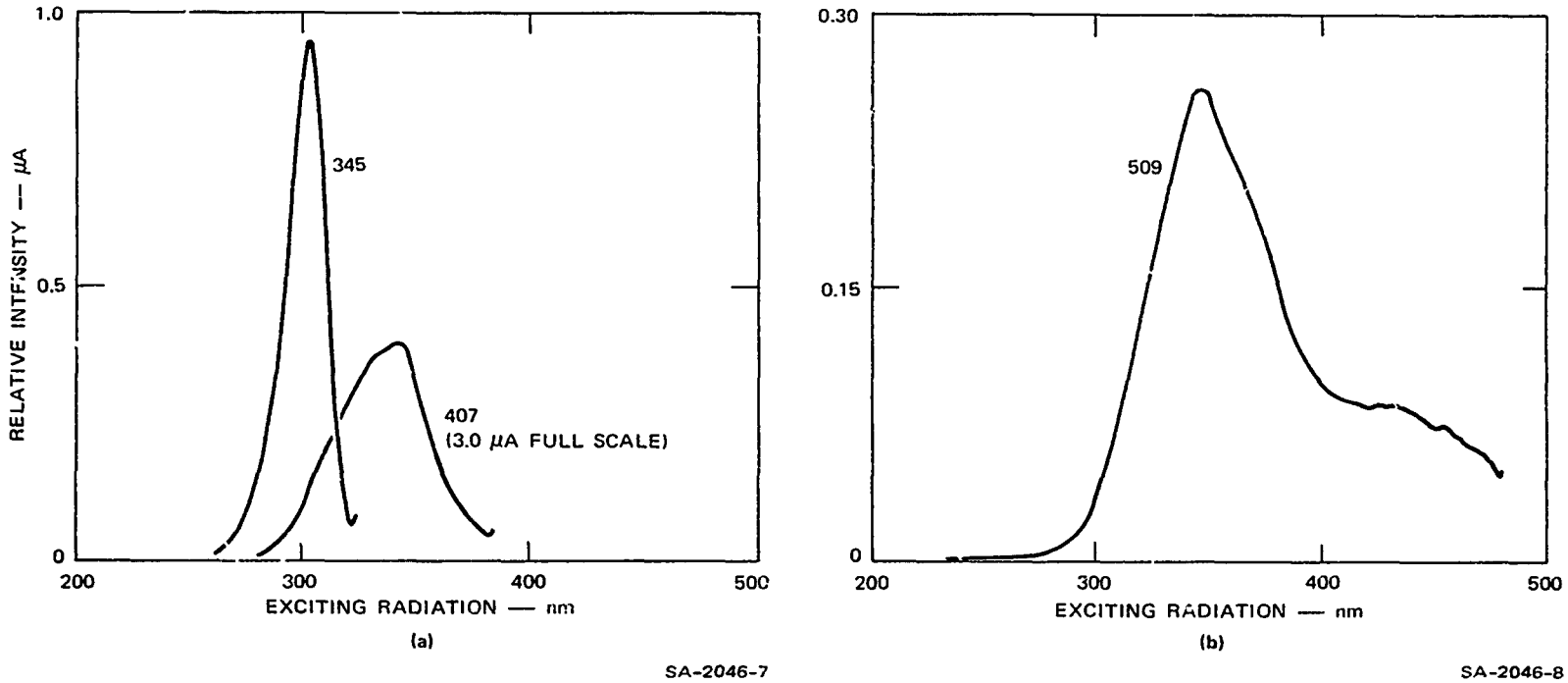

Figure 6 Bacillus subtilis washed and suspended in isotonic saline solution

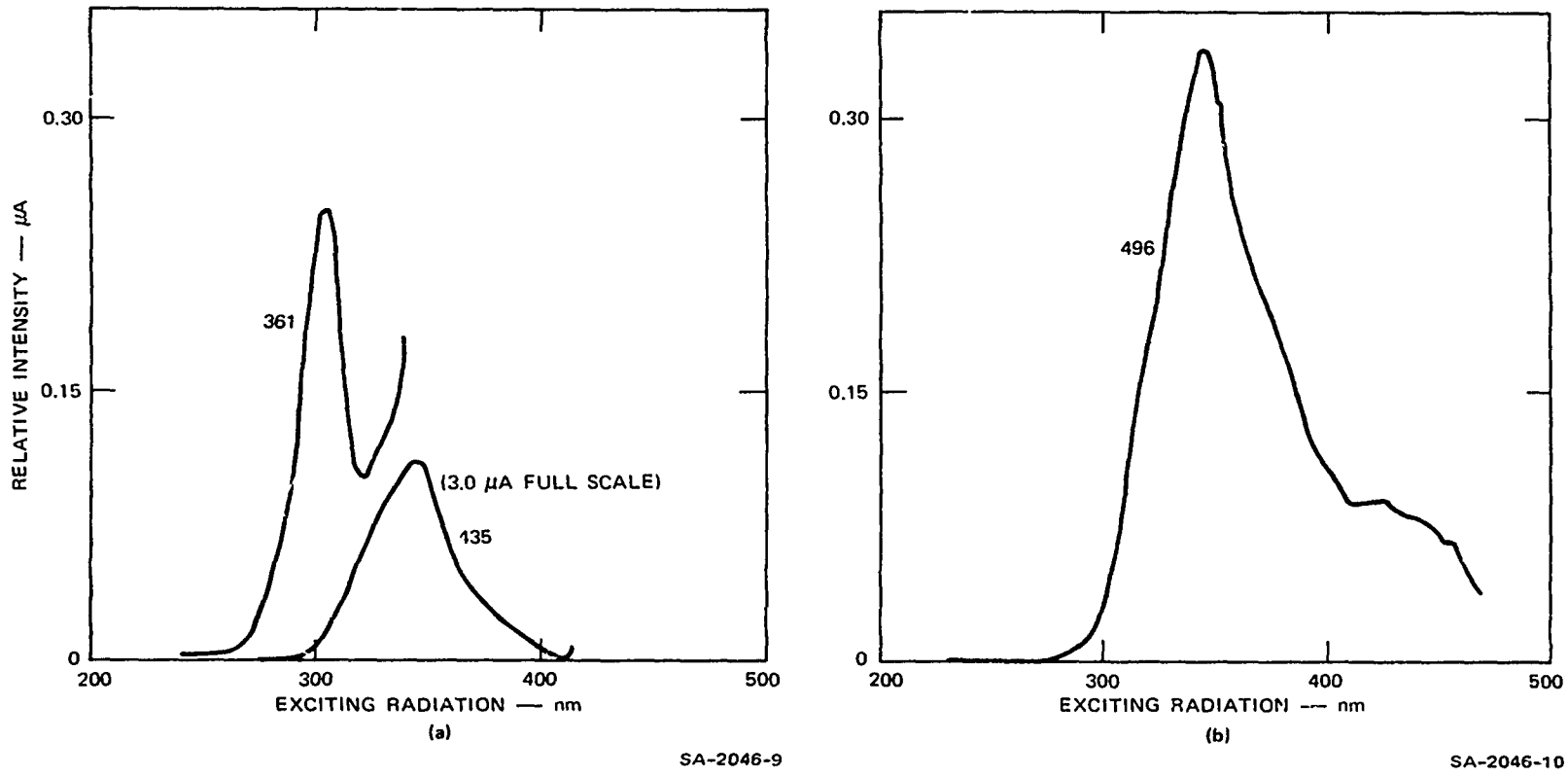

Figure 7 Staphylococcus aureus washed and suspended in isotonic saline solution

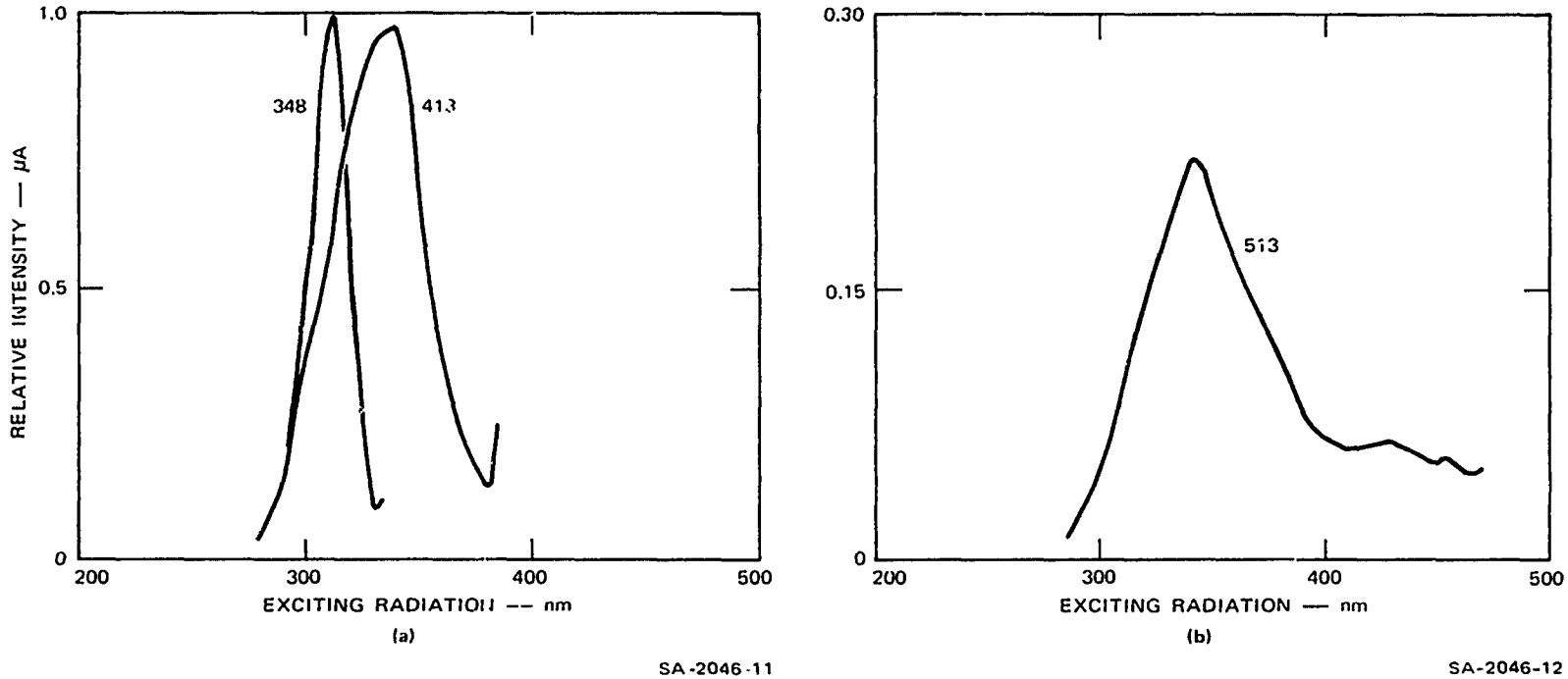

Figure 8 Streptococcus faecium washed and suspended in isotonic saline solution

shown in Figure 4a. There was a decrease in the intensity of the 348-nm response and an increase in the intensity of the 417-nm profile with a significant change at 300 nm. Similar, but not identical, changes in the excitation spectra were observed on heating the same microorganism at 100°C for seven minutes (Figure 4b). Note that the two excitation peaks of the 417-nm fluorescence changed not only in intensity, but also in the relative intensities. It seems that the 417-nm fluorescence is excited by three different chromophores at about 300, 340, and 360 nm.

Unlike E. coli, P. aeruginosa exhibits only the tryptophan fluorescence at 348 nm and undergoes little change on exposure to simulated sunlight (Figure 5a). This microorganism has metabolic products that differ in their fluorescence from those of E. coli (Figure 5b).

B. subtilis exhibits three characteristic fluorescence peaks at 345 nm (tryptophan), 407 nm, and 509 nm (Figures 6a and 6b). S. aureus also has three characteristic fluorescence peaks, but at 361, 435, and 496 nm (Figures 7a and 7b). In this organism, the tryptophan chromophore excited at 295 nm emits its fluorescence at a significantly longer wavelength (361 nm) than that of the other bacteria tested (345 to 348 nm). This shift and the shape of the excitation spectrum indicates a superposition of an additional excitation and fluorescence center in the same spectral region. The other two excitation spectra have shapes similar to those of B. subtilis, although the fluorescence is emitted at significantly different wavelengths (435 versus 407 nm and 496 versus 509 nm).

The next microorganism examined, S. faecium has fluorescence peaks at 348, 413, and 513 nm (see Figures 8a and 8b). The excitation spectra of the 348-nm emission, although similar to those of four other species tested, is significantly shifted, by some 20 nm, toward the longer wavelengths. The excitation spectrum at 413 nm is very much different from that of the 417-nm fluorescence of E. coli, and is similar in general

shape, but not in relative amplitude to the 407-nm and 435-nm fluorescent spectra of B. subtilis and aureus, respectively. Similarly, the third fluorescence peak of faecium at 513 nm has an excitation spectrum very similar to that of the other two gram-positive organisms.

It is hard to tell at this point whether the band fluorescing at 490-510 nm (Figures 6b, 7b, and 8b) is characteristic of gram-positive organisms, but our limited data encourage further experiments in this direction.

3. Polarization Experiments

In several experiments with bulk liquid suspensions, we examined the effect of placing crossed polarizing filters in the exciting light beam and in the path of the emitted fluorescence. This is important information as the ultimate exciting laser beam is highly polarized. The tryptophan fluorescence in all organisms tested decreased in intensity when the crossed polarizers were used. Of the other fluorescence emissions, the 413-nm emission of E. coli displayed an increase in intensity with crossed polarizers, whereas all the other bands of the balance of the organisms showed a decrease. These experiments suggest that polarization may be an additional diagnostic parameter in remote sensing, but more experimental information is required to evaluate its usefulness.

4. Fluorescent Lifetime Measurements

Unlike elastic scatter, absorption, or Raman scattering, fluorescence has a characteristic feature--a relatively long lifetime of the excited state before reemission. Whereas the former processes take place within less than 10^{-4} nsec, fluorescence is emitted 10^{-1} nsec or more following the instance of light absorption. Moreover, some fluorescent materials have excitation lifetimes up to 10^{3} nsec. This

delay in emission has two possible applications. First, one can distinguish between fluorescence and scattering by observing only the light that is returned; say one nsec following a pulse of excitation. Second, as different fluorescent species may have varying lifetimes, this may be used to differentiate between them, in addition to differences in the excitation and fluorescent spectra.

The decay of excited states in complex biological matrices is purely exponential and independent of concentration. This makes the decay time a characteristic parameter. The number of photons collected per unit time from a longer lived excited state will be relatively smaller; that is, longer periods of light integration will be required to obtain the same sensitivity. Thus, if we have two excited species with fluorescence at the same wavelength with half-lives of, say, 5 to 50 nsec, we may integrate all the light between 1 to 20 nsec, and then from 20 to 100 nsec, following the exciting pulse. We would thus collect about 80% of the fluorescence of the first species in the first period, and about 80% of that of the second species in the second period. Now, practically all the residual 20% of the fluorescence of the second species occurs during the first period, whereas 6.25% of that of the first species occurs during the second period. Thus, by easy computation, the real fluorescence of each of the two species can be ascertained.

In view of the potential usefulness of time resolution of fluorescence, we considered different possibilities for determining lifetimes of fluorescent excited states and performed preliminary experiments on our biological substrates.

Two basic techniques have been developed for the measurement of fluorescent lifetimes. The first method[5] is that of phase fluorometry. The fluorescence is excited by a continuous light source, the output of which is modulated at a high frequency by an optical shutter, such as a Kerr cell, or an ultrasonic diffraction grating. The fluorescent

emission output is modulated at the same frequency, but the phase of this output is shifted by an angle that can be related to the fluorescent lifetime by

$$\theta = \tan^{-1} (\omega\tau) \qquad (1)$$

where

θ = the phase difference between the fluorescence and the exciting light

ω = the angular frequency of the modulation

τ = the fluroescent lifetime.

In their present form, phase fluorometers exhibit several drawbacks that could limit their usefulness in the context of this project. The major limitation is that this technique is limited to the observation of fluorescent materials with a simple exponential response function. In principle, it is possible to analyze materials whose fluorescent response is the sum of two exponential decays, by using a series of diverse modulation frequencies, so that the phase variance at different frequencies provides a Fourier transform of the unknown fluorescent response. Fluorometers operating at several frequencies have been constructed,[6,7] but have not been used for the analysis of complex decays.

Because of the possibility of encountering complex fluorescent decays in the materials of interest in this project, the phase fluorometer approach was not considered further.

In single pulse fluorometry, fluorescence is excited by a rapidly pulsed light source of short duration, and the fluorescent lifetime can be observed directly during the interval between excitation pulses. This method requires a pulsed light source whose decay time

is shorter than the expected fluorescent lifetimes, and a detection system with appropriately fast time response.

The fluorescent lifetime of a particular material is defined here as a time τ required for the fluorescence emission to decrease to a value of 1/e from its maximum in response to a Δ function excitation at $\tau = 0$. The modification of the lifetime τ by the fluorometer's instrumental response function is such that the experimentally obtained value of fluorescent lifetime τ_f is usually greater than τ, particularly when working with fluorescent lifetimes in the nsec range.

When the fluorescent response function is exponential, the "method of moments"[8] can be used to obtain τ from the observed value τ_f and from the instrumental decay time τ_i, which is determined from the instrumental response function. If the fluorescent response function, instrumental response function, and observed response function are all approximately exponential, then τ can be determined from the approximate relation

$$\tau^2 = \tau_f^2 - \tau_i^2 \qquad (2)$$

The usefulness of the pulse excitation technique for the measurement of fluorescent lifetime τ is limited by the value of τ_i, which in turn is determined by the decay time of the pulsed lamp, as well as by the response time of the detector, the associated electronics, and display. In the specific case of our preliminary experiments with the Optitron prototype, $\tau_i = 2.9$ nsec.

Figure 9 illustrates typical examples of pulsed fluorometer data. The instrumental response function of the Optitron apparatus is shown in Figure 9a. This waveform was obtained by temporarily increasing the leakage between the excitation and fluorescence channel by inserting a mirror in place of the sample cell. The instrumental decay

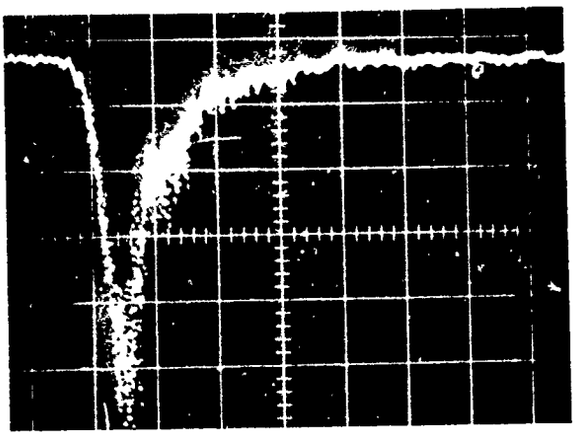

(a) RESPONSE FUNCTION OF THE BASIC INSTRUMENT

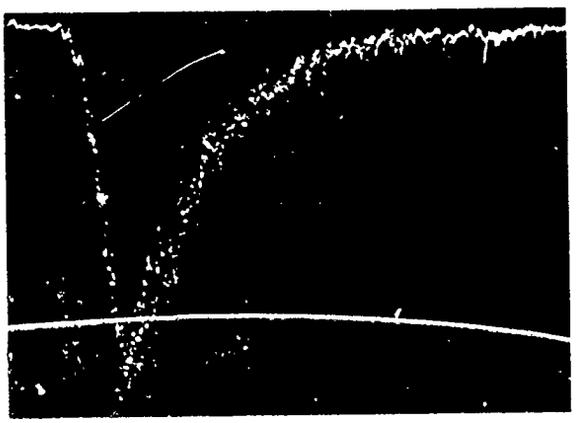

(b) FLUORESCENT LIFETIME OF PSEUDOMONAS

Excitation: 3400 A.

SA-2046-20

Figure 9 Typical examples of pulsed fluorometer data (Time scale 5 nsec/div, vertical scale 50 mV/div)

time τ_i, of 2.9 nsec, was obtained from Figure 10, where the instrumental response function versus time is plotted.

The decay time of the pulsed lamp, 0.3 nsec (1/e value), was measured by means of a high-speed vacuum photodiode and a sampling oscilloscope. This value has been corrected for the fall time characteristics of both the vacuum photodiode and the oscilloscope. The remainder

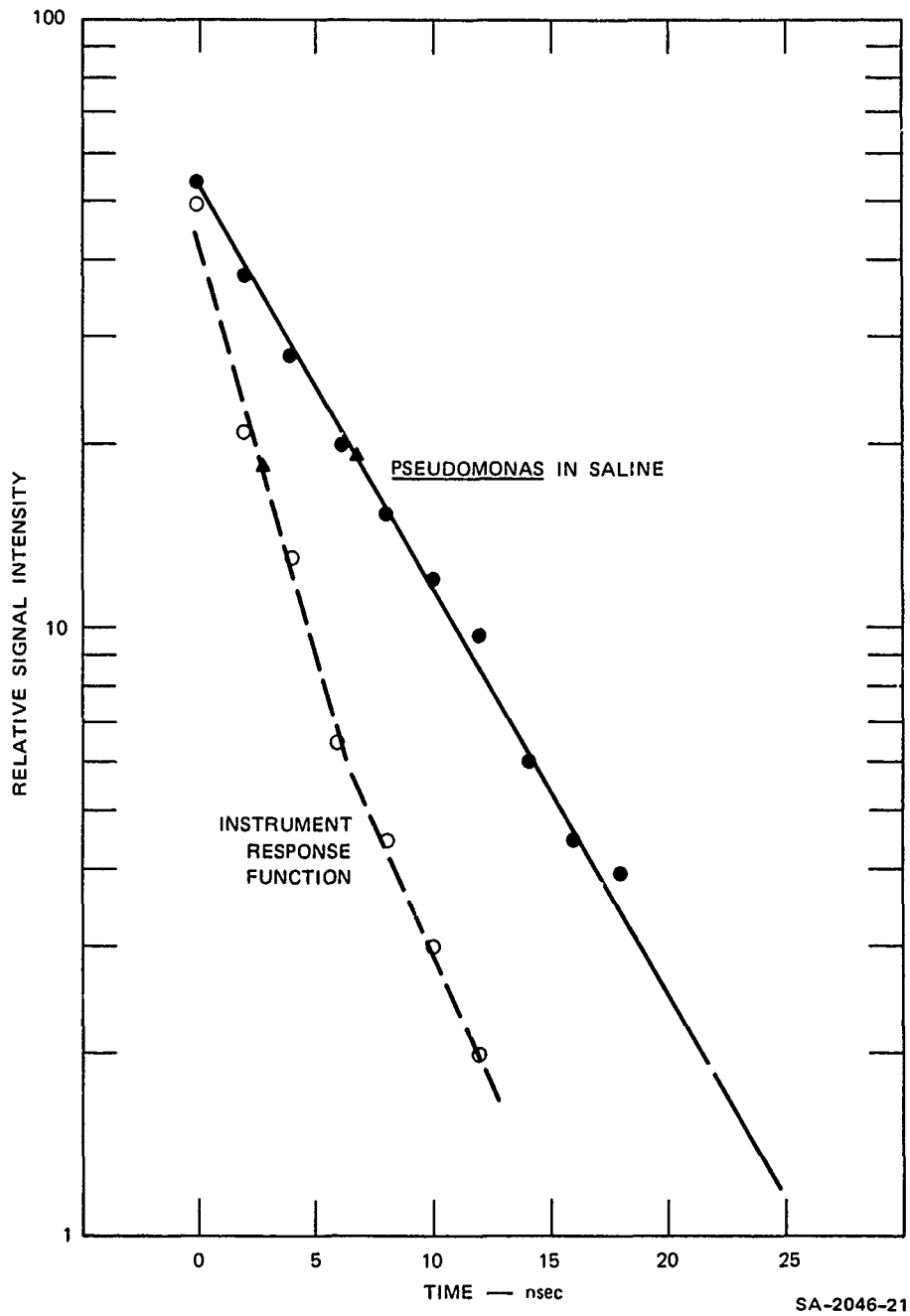

Figure 10 Pulsed fluorometer output versus time

of the decay time of 2.6 nsec is attributed to the photomultiplier (1P28) and the sampling oscilloscope (Tektronix model 564) used to gather the pulsed fluorescence data. Fluorescent lifetimes of several microorganisms and nutrients were obtained using the Optitron instrumentation. Figure 9b shows the fluorescent decay characteristics of P. aeruginosa, excited at 3400 Å. The 1/e fluorescence lifetime (τ_f) of 6.7 nsec was determined from a plot of fluorescence intensity versus time in Figure 10. The fluorescent lifetime τ was calculated to be 6.6 nsec using Equation (2).

Using these experimental techniques, the fluorescent lifetime of nutrient is approximately 5 nsec, and the 1/e fluorescent lifetime of the 4070 Å band in B. subtilis is about 10 nsec.

Although the difference in the organism fluorescent lifetimes is longer just by a factor of two, it is long enough for time resolution analysis. Let us say that we integrate the light received between 10 and 20 nsec following the pulse, and then between 30 and 150 nsec. The fluorescence collected during the second interval (F_2) will then include 25% of the fluorescence of the microorganisms and only about 7% of the fluorescence of the nutrient. Corresponding fluorescence of the first interval (F_1) will include 25% of the fluorescence of the organisms and about 18% of the nutrient. Thus, if the ratio $(F_1 - F_2)/F_2 \geq 1$, the presence of a long-lived fluorescent species is excluded. In the presence of microorganisms and a comparable fluorescence of nutrients, $(F_1 - F_2)/F_2$ will be smaller than unity.

It is possible that other fluorescent states for the microorganisms will have significantly longer lifetimes. With the Optitron equipment, we have been unable to obtain adequate time resolution data on the tryptophan peak for several organisms, because of the proximity of the excitation and fluorescence wavelengths and the general unavailability of the proper filters in the 300-nm region. However, suitable

filters may be specially ordered if it is decided to pursue this investigation in follow-on work.

5. Bacterial Aerosols

The fluorescence of aerosols of E. coli and P. aeruginosa were studied using isotonic saline suspensions of approximately 1.3×10^9 organisms/ml. Figure 11 presents the fluorescence at 350 nm of an aerosol of E. coli. The fluorescent response from the aerosol was about a factor of 20 lower than obtained from the bulk liquid samples, and in this case the spectrometer was operated at unusually high sensitivities. We obtained an instrumental background reading using a distilled water aerosol. As can be seen in the figure, the baseline in this case is not flat, but peaks in the same region as does the band for the organism. It was thus necessary to subtract the fluorescent spectrum from the scattering background of distilled water (Figure 11a) to obtain the corrected excitation spectrum (Figure 11b). The corrected spectrum is qualitatively similar to that of the same microorganism in aqueous suspension (Figure 3a). It was on the basis of these positive results that we embarked subsequently on a study of remote aerosol detection (Phase II), as described later in this report.

The metabolic products from P. aeruginosa are highly fluorescent (Figure 5b), and a spectrum from an aerosol of these organisms was readily obtained (Figure 12). In this case the scattering background for distilled water is essentially flat.

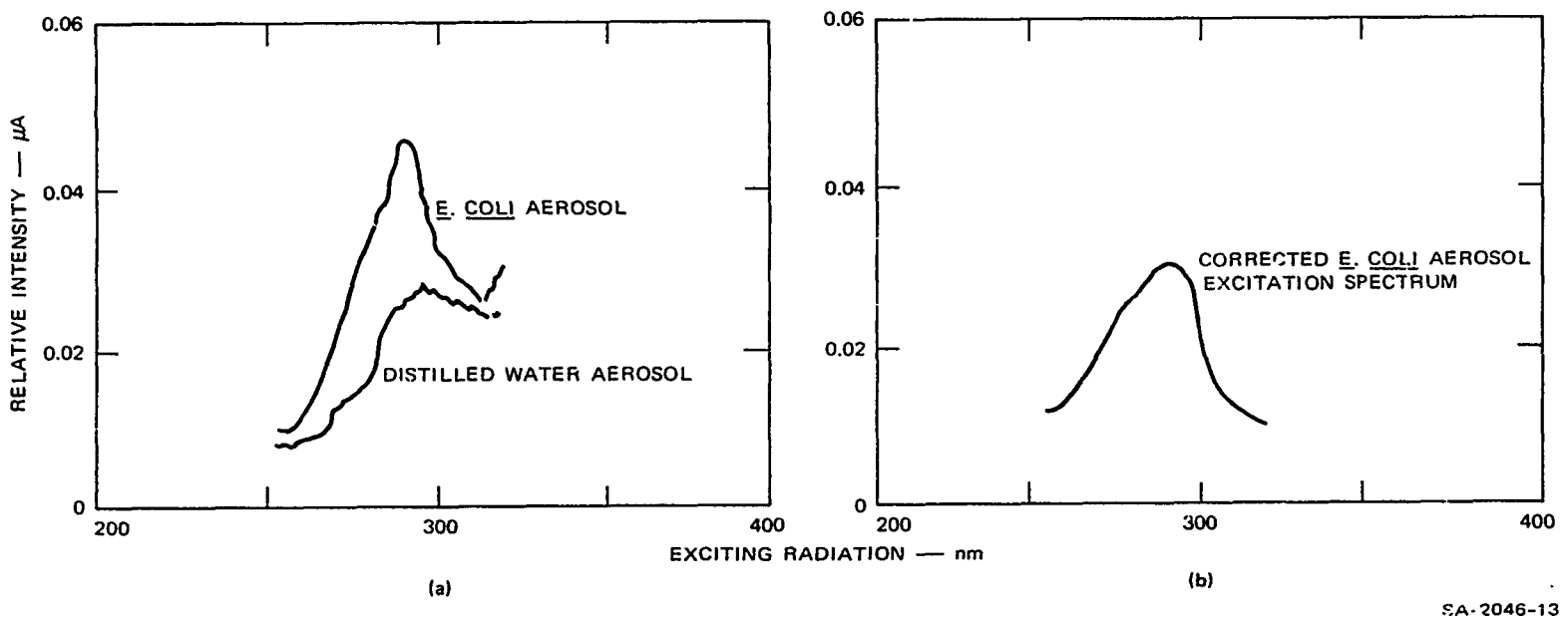

Figure 11 Excitation of E. coli aerosol with distilled water aerosol as reference, followed at 350 nm The organism density in the reservoir was 3×10^9 cells/ml.

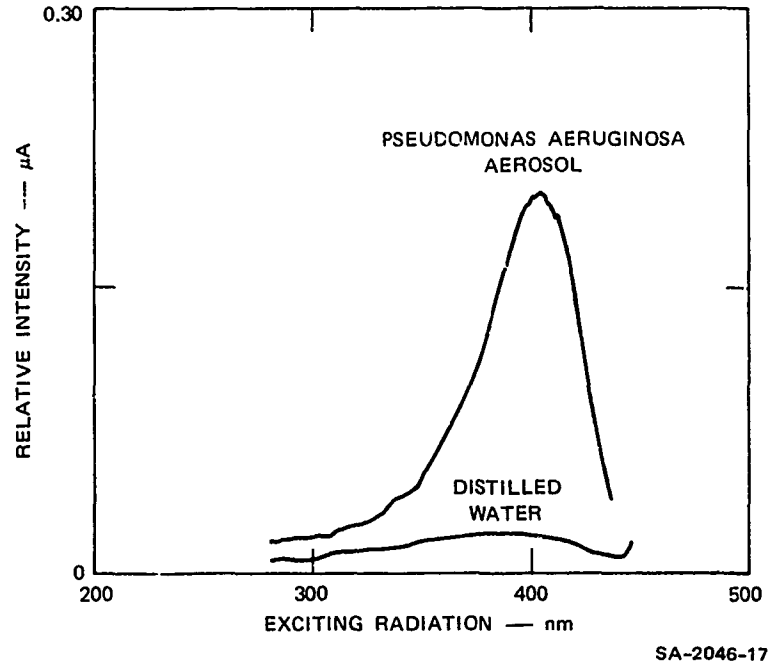

Figure 12 Excitation of P. aeruginosa aerosol with distilled water aerosol as reference, followed at 475 nm

The organism density in the reservoir was 1.8×10^9 cells/ml.

6. Quantum Yield Measurements

Both the excitation and fluorescence channels of the fluorometer were calibrated to obtain quantum yield estimates of the fluorescent aerosols. This information was used to make preliminary assessments of potential range performance of remote detection systems that utilize fluorescent techniques.

The spectral intensity of the illumination incident on the fluorometer sample cell was measured by means of an optical power meter whose calibration is traceable to NBS standards. The raw data shown in Figure 13 are corrected for the spectral sensitivity of the detector and for the spectral reflectivity of a mirror used in the measurement

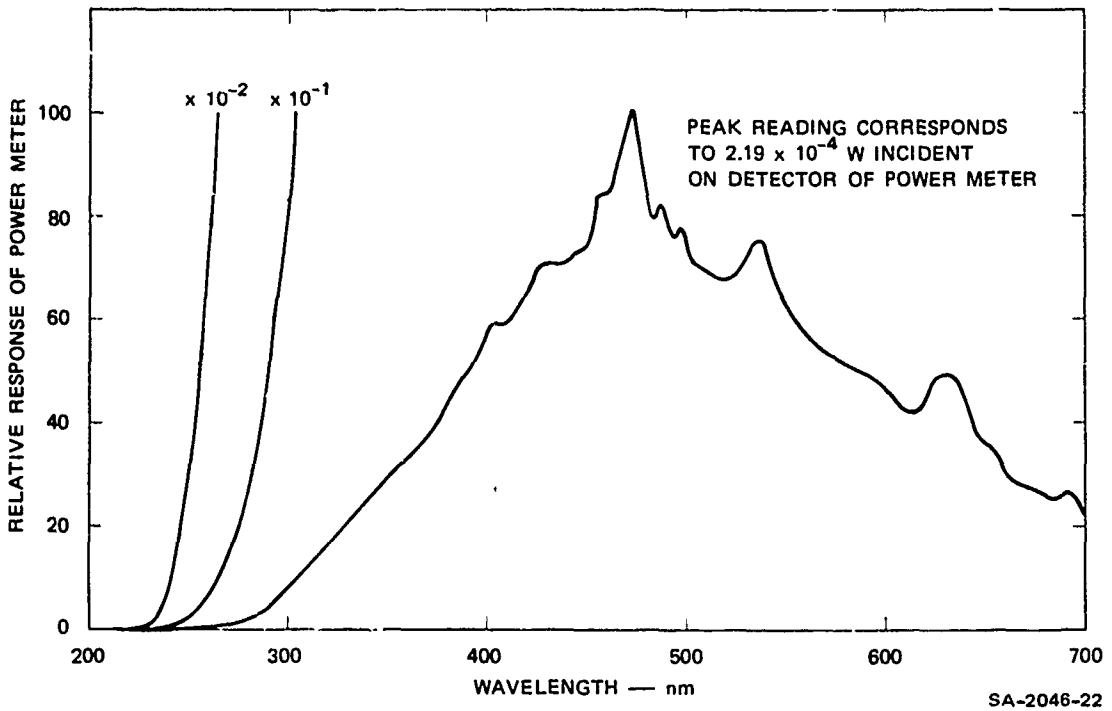

Figure 13 Relative spectral intensity of illumination incident on fluorometer sample cell (uncorrected for detector response)

technique. The final data are in the form of number of quanta per second incident on a fluorometer sample cell as a function of wavelength.

The fluorescence channel was calibrated by a similar optical geometry, using a standard lamp whose spectral irradiance is accurately known. The raw data (Figure 14), in the form of photomultiplier anode current as a function of wavelength, were corrected for the spectral irradiance properties of the lamp and for the spectral transmission of a neutral density filter used in the measurement. The final data are in the form of number of quanta per second incident on the fluorescence monochromator input slit as a function of wavelength.

These two calibrations are valid only as long as neither excitation nor fluorescence channels of the fluorometer experience any significant drift in their respective calibrations. The performance

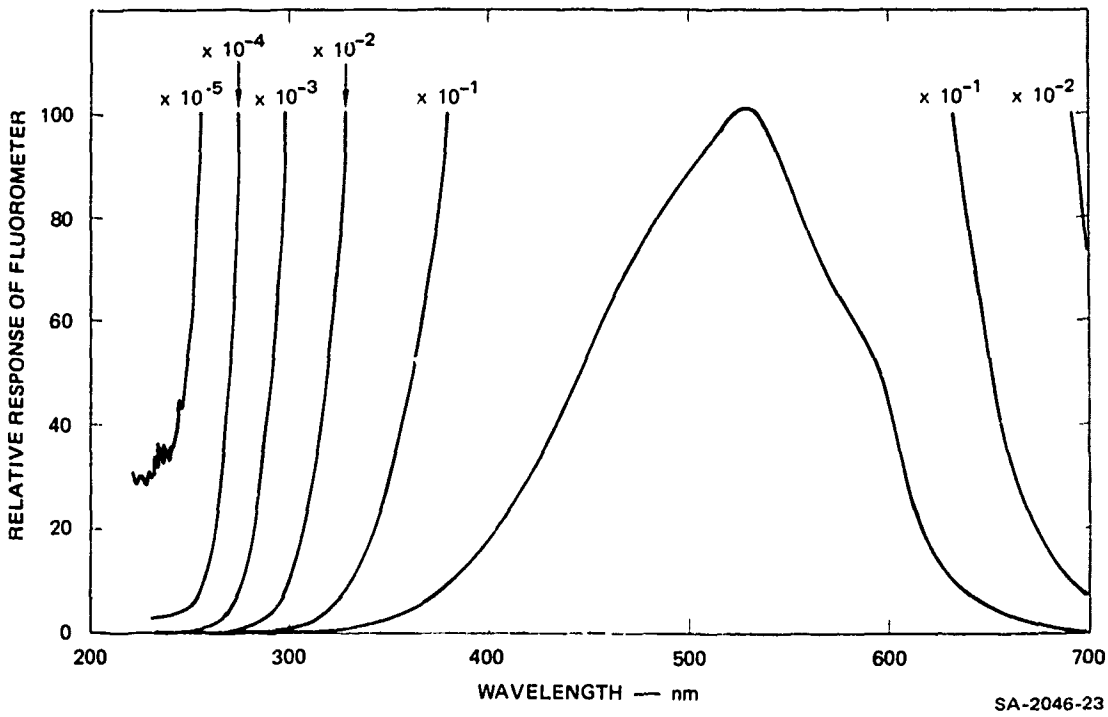

Figure 14 Relative spectral response of fluorometer detector to 3000°K black body source

monitoring techniques described previously are capable of detecting any significant change in fluorometer performance.

7. Preliminary Calculations of Range Performance

Preliminary range performance calculations may be made at discrete wavelengths based on excitation and fluorescence intensity data of the microorganisms in the aerosol state.

The fluorescence intensity of aerosolized P. aeruginosa measured at 473 nm, was 220 nanoAmperes (nA) at the maximum of the band. From calibration data, an excitation monochromator wavelength setting of 400 nm will produce a photon flux of 1.12×10^{14} quanta/second incident on the sample cell. At a fluorescence monochromator wavelength setting of 473 nm, 220 nA of average anode current corresponds to a photon flux of 1.25×10^{7} quanta/second incident on the monochromator slit (1 nm path length), which corresponds to an isotropic photon flux of 7.7×10^{8} quanta/second. These values have been determined by an absolute measurement of the photomultiplier current at given wavelength and geometry, using the standard NBS light source with its calibrated black body spectrum.

From the organism concentration in the nebulizer reservoir (1.8×10^{9} org/ml of bulk liquid), nebulization rate (3 ml/min), flow rate (450 ml of air/min), and volume for a 5 μm-diameter particle (6.5×10^{-11} ml/particle, the following characteristics are derived:

Particle concentration = $3/(6.5 \times 10^{-11} \times 450) = 1.0 \times 10^{8}$ particles/ml of air.

Organism concentration = $(1.8 \times 10^{9} \times 3)/450 = 1.2 \times 10^{7}$ organisms/ml of air

Total mass concentration (for liquid density of 1 g/ml) = 3/450

$= 6.67 \times 10^{-3}$ g/ml of air

$= 6.67 \times 10^{3}$ g/m^3

For a concentration of 1 mg/m^3 and 1 mm path length, the isotropic photon flux would thus be 1.15×10^{2} quanta/second. If the isotropic fluorescence yield is defined as number of emitted phototons per number of incident photons, then the isotropic fluorescence yield at a standard concentration of 1 mg/m^3 is $1.15 \times 10^{2}/1.12 \times 10^{14} = 1.03 \times 10^{-12}$ per mm path length.

Assume a laser pulse 4.5 m long in space (pulse width 30 nsec) with an energy of one joule at 400 nm (2×10^{18} photons) in a beam 1

m^2 in area incident on a cloud of 1 mg/m^3 concentration. The resultant fluorescent emission (Q_f) would be:

$$(2 \times 10^{18})\ (4.5)\ (10^3)\ (1.03 \times 10^{-12}) = 9.27 \times 10^9 \text{ quanta} \quad (3)$$

Assuming an optical radar with a receiver aperture (Ar) of 0.07 m^2 (30 cm in diameter) and a detection sensitivity (Qmw) of 10 quanta, the maximum range is:

$$R_{max} = \left[\frac{(Q_f)(Ar)}{4\pi\ Qmw}\right]^{1/2} = 2.27 \text{ km} \quad (4)$$

This calculation is for a coaxial emission and reception geometry, which does not allow efficient time resolution measurement. If time resolution is required, the emitter and receiver have to be separated by 20 m or more and the observed volume would be reduced to 1 m^3. Such an arrangement would also require somewhat shorter pulses, say, 10 nsec in length. Using the ruby laser, one would obtain only about half the energy output per pulse, and the effective range would then decrease by a factor of 3, to 750 m. To bring up the range to 2.25 km, we would have to triple the energy output (which is feasible), or use a receiving telescope with a diameter of 50 cm (which is also feasible).

The quantum field measurements were based upon calculated values of aerosol concentration within the spectrofluorometer flow cell. The calculated concentration represents an upper bound of the aerosol concentration within the flow cell, because of a number of mechanical effects such as agglomeration, wall effects within the vertical column connecting the aerosol generator and the flow cell, possible preferential nebulization of the saline and not of the organisms, and the like. Accordingly, the use of this upper-bound estimate of aerosol concentration would yield conservative estimates of maximum detection range for a remote detection optical sensor.

While it is true that the fluorescence radiation is isotropic, the field of view of the fluorescence monochrometer was precisely defined by its entrance slit. The beam dimension of the excitation monochromator output incident on the flow cell was taken into account when calculating quantum yield, as was the field of view of the fluorescence monochromator.

A major disadvantage of virtually all spectrofluorometers is that the resulting excitation and fluorescent spectra are heavily biased by the optical characteristics of the individual fluorometer. This machine-dependent bias is also wavelength dependent, so that meaningful comparison of spectra of identical samples taken on different spectrofluorometers cannot, in most cases, be accomplished.

To make comparisons of spectra, the aforementioned machine-dependent bias must be removed. This correction could be accomplished by the use of an absolute spectrofluorometer (such as the type manufactured by Turner, Inc., Palo Alto, California), or by the optical calibration of both the excitation and fluorescence paths of a conventional spectrofluorometer. These calibrations are then used to normalize the excitation and fluorescent spectra.

The apparatus used in these experiments was no exception to the above situation. In the initial estimates of feasibility the spectra of P. aeruginosa was corrected by the experimentally derived instrumental transfer functions of Figures 13 and 14. These corrections were applied at the specific wavelengths of interest. Absolute numerical corrections for comprehensive comparisons with data from other instruments would require considerably more effort than that required for this feasibility study.

8. Aerosol Diffusion Model

In our proposal for this research we discussed the possiblity of using the particle size distribution of the aerosol as a function

of time to determine its residence time in the atmosphere. Particle sizes can be estimated from backscattering, especially if observed at two wavelengths. This information will be available to us if we use a ruby laser with a doubling element, which emits both the fundamental photons plus the double energy photons. We have, therefore, carried out an analysis of an aerosol diffusion model, which gives us an idea of size distribution as a function of location and time.

The behavior of a cloud of particles from an instantaneous, cross-wind line source is often described by a Gaussian formulation of the following form:[9]

$$\chi = \frac{Q}{(\pi\sigma_{xI}\sigma_{zI}} \exp\left\{-\frac{1}{2}\left[\left(\frac{x'}{\sigma_{xI}}\right)^2 + \left(\frac{z'}{\sigma_{zI}}\right)^2\right]\right\} \qquad (5)$$

where:

χ = concentration (No. m^{-3} or g m^{-3})

Q = strength of the instantaneous line source (No. m^{-1} or gm m^{-1})

σ_{xI}, σ_{zI} = standard deviations of the Gaussian concentration distribution in the along-wind and vertical directions (m)

x', z' = distance from cloud center in along-wind and vertical directions (m).

The standard deviations, σ_{xI} and σ_{zI}, are functions of atmospheric stability and the distance (or time) that the cloud has traveled downwind since release.

If we choose to treat a cloud of particles with finite settling velocities, then certain further assumptions are required. Assuming that average motions transporting all particles of the same size are the same as those at the center of the cloud, then the whole cloud will

be settling at a rate corresponding to the terminal velocity, v_T ($m\ s^{-1}$), and

$$z' = z - (H - v_T t) \tag{6}$$

where:

z = height (m)

H = the original height of release (m)

t = time since release (sec).

The term $(H - v_T t)$ represents the height of the center of a cloud of particles, all with a settling velocity of v_T; that is, all the same aerodynamic size. If the wind speed varies with height, these settling particles will be subjected to different downwind transport rates, and the center of such a cloud will be at a different downwind distance from a nonsettling cloud released at the same time and place. In the following derivation, the assumption is again made that the whole cloud of particles of a given size moves with the center of that cloud.

If the variation of average wind speed (normal to the line of release) is given by f(z), then the horizontal displacement x_c of the cloud center relative to the center of a nonsettling cloud is given by

$$x_c = \int_0^T f(H - v_T t)dt - \bar{u}_H T \tag{7}$$

where:

$\bar{u}_H$ = component of the average wind normal to line source at release height, H

T = total travel time of the cloud (sec).

The distance from the center of the cloud, x', is given by

$$x' = x - x_c \tag{8}$$

where both x and x_c are along-wind distances measured relative to the center of the nonsettling cloud.

The following is a good first approximation of $f(z)$[10]

$$\bar{u} = f(z) = \bar{u}_H \left(\frac{z}{H}\right)^p \tag{9}$$

Substitution in equation (7) gives:

$$\begin{aligned} x_c &= u_H \left[\int_0^T \left(\frac{H - v_T t}{H} \right)^p dt - T \right] \\ &= u_H \left\{ - \frac{H}{(p+1) v_T} \left[\left(1 - \frac{v_T}{H} T \right)^{p+1} - 1 \right] - T \right\} \end{aligned} \tag{10}$$

For particles whose settling velocities are large enough to be of importance, Stoke's settling equation can be used to calculate v_T for unit density spheres in air:

$$v_T = \frac{2gr^2 \rho}{9\nu} = 1.15 \times 10^8 \, r^2 \text{ m sec}^{-1} \tag{11}$$

where

g = acceleration of gravity (9.8 m sec^{-1})

r = particle radius (m)

ρ = particle density (assumed 1 g cm^{-3} = 10^3 kg m^{-3})

ν = viscosity of air (1.9×10^{-5} kg m^{-1} sec^{-1})

Equations (6), (8), (10), and (11) can be used to determine the appropriate values of x' and z' for use in Equation (5) for a given particle size. If the total mass or number loading is desired, then Equation (5), with appropriate substitutions, must be integrated over the entire spectrum of particle radii, r:

$$\chi = \frac{Q}{\pi \sigma_{xI} \sigma_{zI}} \int_0^{\infty} \left\{ F(r) \exp \left[-1/2 \left(\frac{x'(r,t)}{\sigma_{xI}} \right)^2 - 1/2 \left(\frac{z'(r,T)}{\sigma_{zI}} \right)^2 \right] \right\} dr \qquad (12)$$

where

Q = the total source strength (No. m^{-1}, or g m^{-1})

$F(r)$ = normalized initial particle-size distribution (fraction/radius interval, m^{-1}).

For modeling purposes, a log-normal particle size distribution has been chosen, i.e.,

$$F(r) = \frac{1}{\sqrt{2\pi}\ r \ln \sigma_g} \exp \left\{ -1/2 \left[\frac{\ln (r/\bar{r}_g)}{\ln \sigma_g} \right]^2 \right\} \qquad (13)$$

where:

$\bar{r}_g$ = geometric mean radius (m) of the particles released.

σ_g = geometric standard deviation.

If the integration in Equation (13) is carried out over the interval

$$\bar{r}_g / \sigma_g^3 \leq r \leq \sigma_g^3 \bar{r}_g \qquad (14)$$

then more than 99% of the material will be accounted for.

The model calculates concentrations of settling particles, emitted initially as an infinite crosswind line source with log-normal size distribution and a power law wind profile. It consists of Equations (6), (8), (10), (11), (12), and (13) and a trapezoidal integration of Equation (12), using 200 increments over the interval defined by the inequality (14).

The size distributions at various locations and times can be determined from the integration of Equation (12) over intervals less than the entire range of sizes, and normalized according to the total amount of material.

The model described above has been programmed for computer use and applied to two specific cases for purposes of illustration. In both cases, the meteorological conditions are the same; the two cases differ only in the size distribution of the material released. Table 4 shows the values of the parameters used for the calculations. The meteorological parameters are typical of neutral atmospheric conditions.

For the size distribution used in Case 1 (see Table 4), the particles are small, settling proceeds only very slowly, and the highest concentrations occur very near the release height. The asymmetry is very slight, as can be seen in Figure 15. In Case 2 with its larger particles, settling is appreciable, and greatest concentrations appear well below the release height, see Figure 16. The larger particles, having fallen to regions of lower wind speed, have not traveled as far, so there is a tendency for the cloud to lag behind where it would be if transported by release height. Had it traveled at that wind speed, its center would be 900 m downwind.

As noted earlier, settling particles will cause variations in the particle distributions in different parts of the cloud. The largest

TABLE 4: PARAMETERS USED IN MODELING CONCENTRATIONS FROM AN INSTANTANEOUS LINE SOURCE

Release height, H	300 m
Source strength, Q	1 g m^{-1}
Cross-wind speed at release height, $\bar{u}_{300}$	3 m sec^{-1}
Exponent in wind profile, p	0.35
Time since release, T	300 sec
Lateral standard deviation, σ_{xI}	30 m
Vertical standard deviation, σ_{zI}	25 m
Mass median radius, $\bar{r}_g$	3×10^{-6} m (Case 1)
	25×10^{-6} m (Case 2)
Geometric standard deviation, σ_g	1.7 (Case 1)
	2.0 (Case 2)

particles will tend to be below and behind where the center of the cloud would be if no settling took place. For the small particle case (Case 1), the differences are very small, but for the larger particles (Case 2), the difference can be appreciable. Figure 17 shows the cumulative size distributions at two locations in the cloud that have similar mass concentrations, both about 90 $\mu g\ m^{-3}$. These two size distributions are quite different, e.g., the mass median diameters differ by a factor of about two and one-half, as shown in Figure 17, they also differ substantially from the size distribution of the particles as originally released.

A model of the type discussed here could provide a basis for analyzing observed concentrations in the field. The linear nature of the cloud, as observed by lidar or other means, would usually distinguish

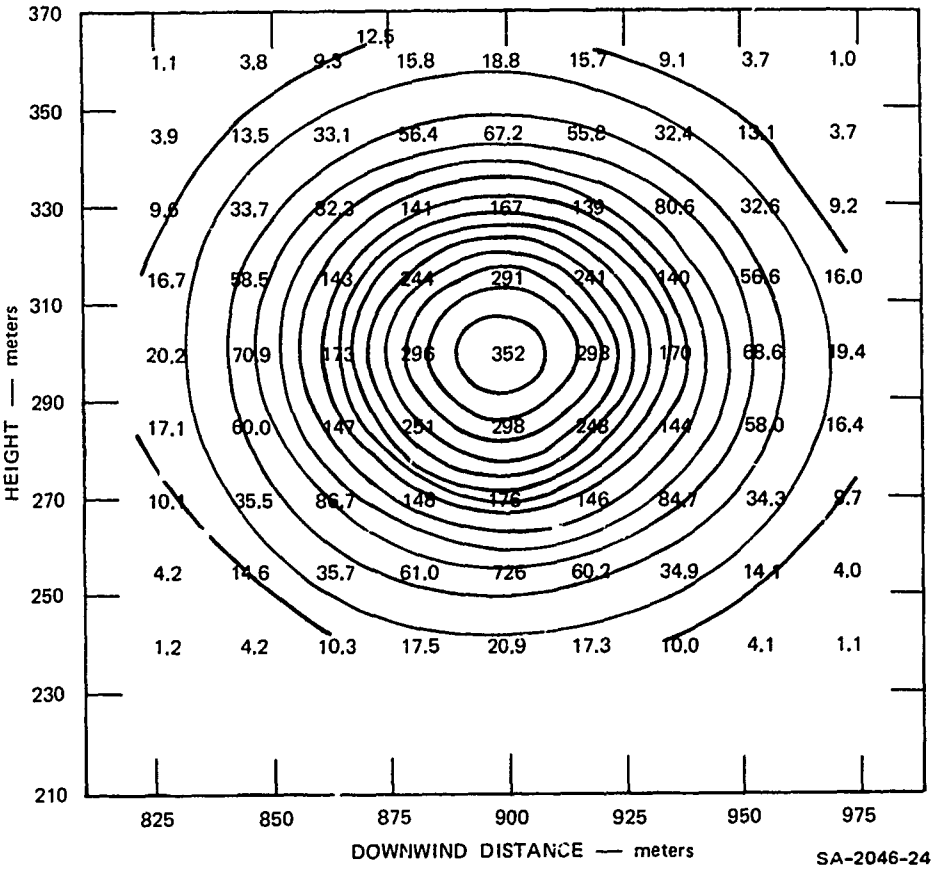

Figure 15 Mass concentrations (μgm m^{-3}) for line release—Case 1

an artificial cloud from a natural one. Distribution of concentrations and sizes would be very indicative of the nature of the material originally released, particularly if changes in these distributions with time were observable. This kind of model also provides a valuable method for generating expec conditions for theoretical studies.

9. Discussion and Summary of Results--Phase I

The primary purpose of the laboratory experiments was to:

(1) Obtain the excitation and fluorescent spectra of a small number of selected microorganisms, both in bulk liquid suspension and in aerosol form.

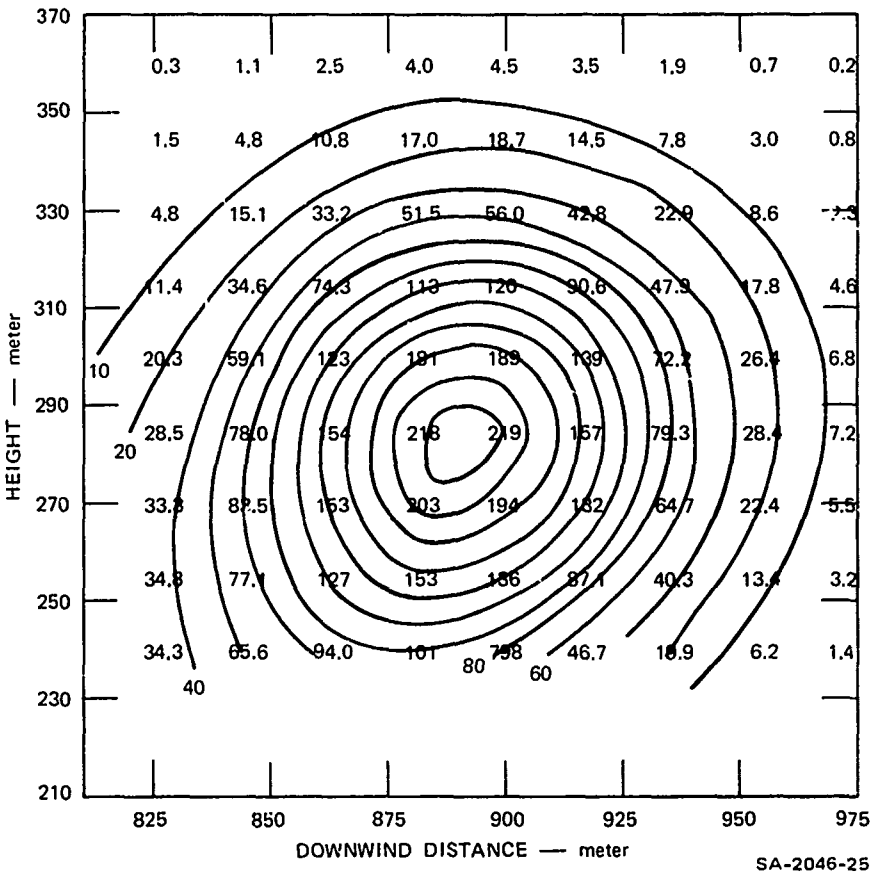

Figure 16 Mass concentrations ($\mu gm\ m^{-3}$) for line release—Case 2

(2) On the basis of these data, estimate the performance of a hypothetical optical sensor operating in a realistic atmospheric environment.

Secondary objectives include:

(1) Investigating the chemical and physical processes that accompany aging of aerosols.

(2) Determining whether these aging effects could significantly modify the optical properties of the aerosol.

(3) Investigating the potential usefulness of other optical properties associated with the fluorescent effect (such as fluorescence lifetimes and polarization effects).

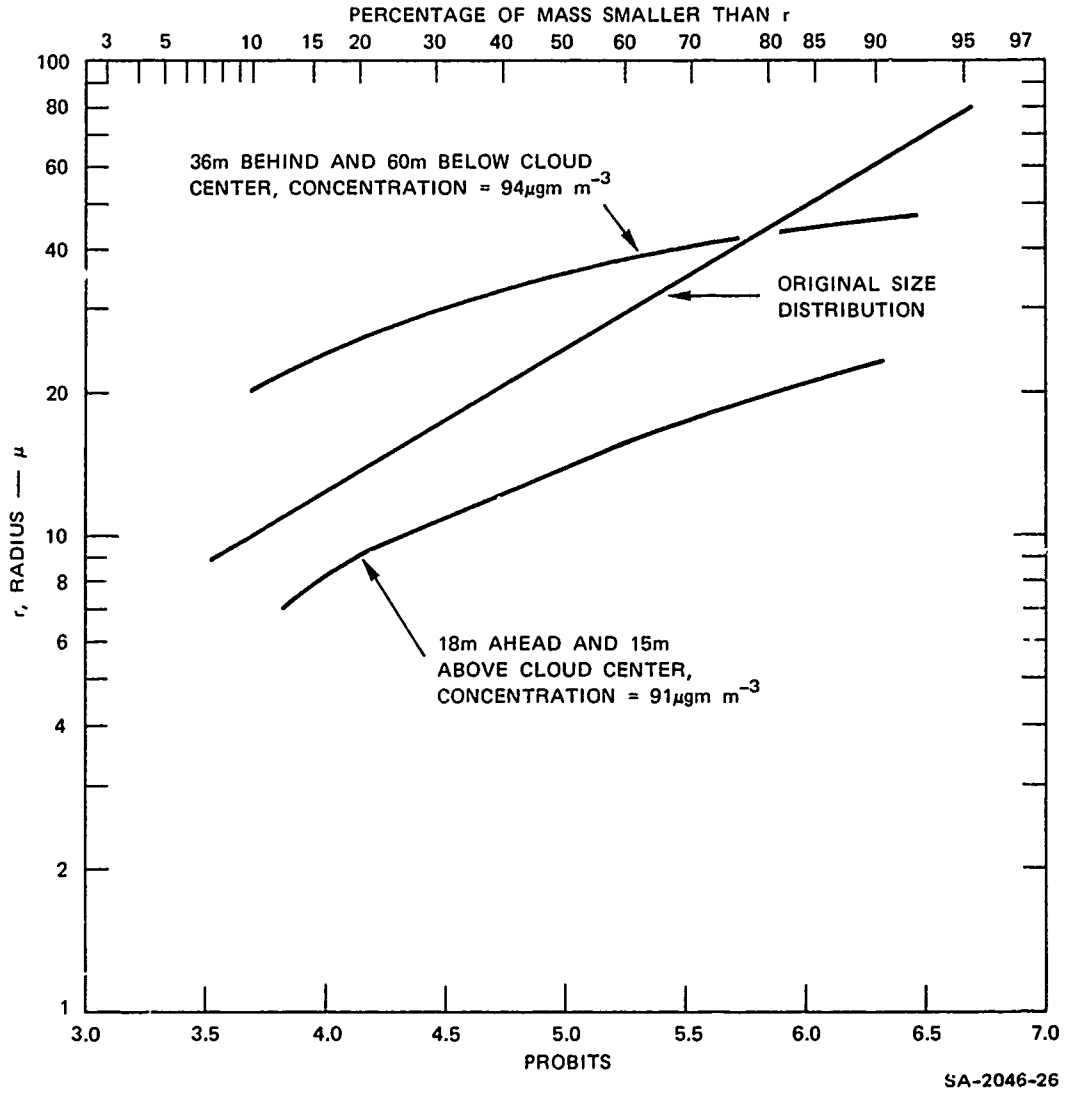

Figure 17 Size distributions at different locations in the cloud—Case 2

The laboratory measurements have established that E. coli and P. aeruginosa in aerosol form exhibit characteristic excitation spectra. These measurements, made at sea-level temperatures and pressures, indicate that fluorescence quenching effects do not appear to inhibit significantly the fluorescence mechanism, although quenching may be present to some degree.

Performance calculations of a hypothetical optical sensor were made, based on data obtained from an analysis of the laboratory measurements. These calculations indicate that detection range in the order of 1-2 km could be ultimately achieved at sea-level, midlatitude geographical locations.

Fluorescent spectra of organisms often are composed of characteristically broad, featureless bands of little diagnostic use. However, we have found that the excitation spectra are typically sharper and show detailed structure in some cases. This feature, if unique, could be utilized to improve the specificity of the sensing system by rejecting the returns from nonviable aerosols.

The tryptophan peak (excitation $\approx$ 3000 Å, fluorescence $\approx$ 3500 Å) appeared in all bacterial spectra. This peak appears to be a distinguishing feature of organisms and could also be used to increase the specificity of the optical sensing system.*

Organism suspensions, subjected to aging by means of artificial sunlight, exhibited some change in their characteristic excitation spectra although some organisms produce larger changes than others.

Physical changes of an aerosol cloud, such as changes in particle size distribution resulting from gravitational settling can be significant for aerosols with mass median diameters greater than about 25 microns. In such situations, the particle size distribution (and the lidar reflectivity) will show significant differences as a function of time and of vertical location within the cloud. However, for smaller particle sizes (for example, mass median diameter 6 μm), the differences

---

*In some preliminary screening work, it was observed that, for a small number of yeasts, the tryptophan peak was absent.

in particle size distribution as a function of time or height tend to be very small.

The polarization properties of several organisms in bulk liquid suspension were examined in the spectrofluorometer. Although most measurements indicated an 80-90% depolarization of the fluorescent radiation, several intriguing effects were noted. For a given organism suspension, some excitation bands show total depolarization; other bands of the same organism show a strong polarization with very little rotation; and still other bands of the same organism show strong polarization with approximately 90° rotation.

Fluorescent lifetimes of several organisms were measured at the peak of their respective excitation and emission bands. The 1/e fluorescent lifetime of P. aeruginosa was measured at 6.6 nsec and the lifetime of B. subtilis was measured at 10 nsec. The decay time of the tryptophan band could not be measured at this time because of the general unavailability of optical filters with the required characteristics.

IV PHASE II--REMOTE DETECTION EXPERIMENTS

A. Introduction

To verify the conclusions reached during the laboratory experiment phase of this program, a series of remote detection experiments were conducted. These experiments involved the use of two major pieces of equipment: the Mark IX lidar facility (suitably modified for fluorescence work) and an aerosol target volume confined within a vertical column, which was located 90 meters away from the lidar.

The objectives of these experiments were to:

(1) Demonstrate the basic principle of remote fluorescence detection under simulated field conditions.

(2) Obtain experimental data that would be used to verify the conclusions reached during the laboratory experiment phase of the program.

(3) Using the experimental data as a basis, extrapolate the performance of the experimental equipment to remote fluorescence sensors specifically designed for this application.

B. Experimental Apparatus

A sketch of the overall experimental configu tion is shown in Figure 18. The specific site for the experiment was selected primarily because of the availability of an existing tower structure located near SRI laboratory buildings. This tower structure formed an integral part of the aerosol column which was subsequently constructed within the structure.

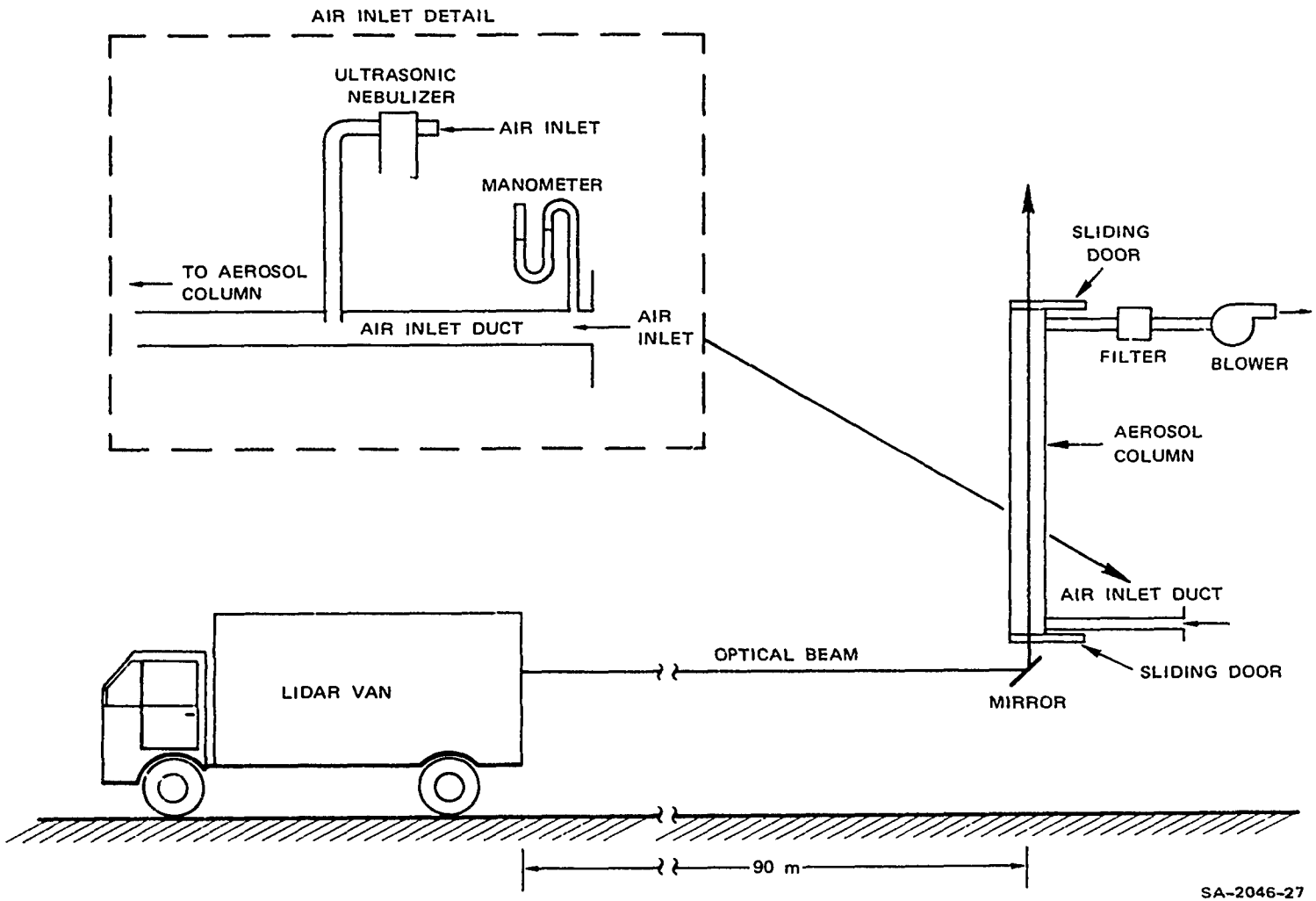

Figure 18 Configuration for the remote sensing experiments

The optical van (Figure 19) containing the modified lidar was located 90 meters from the column (Figure 20). The lidar beam was transmitted from the van along a horizontal path toward a mirror located at the base of the aerosol column. This 45° mirror deflected the beam vertically into the aerosol column, and then into the atmosphere. The field-of-view of the optical receiver was oriented along an identical path, the receiver thus being able to receive both the elastic scattered return from the aerosol cloud within the column and the fluorescent return.

C. Aerosol Column

The aerosol column consisted of a vertical cylinder 0.6 m (2 ft) in diameter and 6 m (20 ft) long (Volume: 1.8 m^3), the lower end of the column being 1.8 m (6 ft) above the ground. The top and bottom of the column were closed by horizontal sliding doors, controlled remotely from the lidar van. The first surface mirror was located immediately beneath the sliding door at the lower end of the column. The decision to use sliding doors on the chamber was made after it was determined that optical parts would have required expensive antireflection coatings. Lidar backscatter signals were not noticably influenced for up to 10 seconds with the doors open.

Air at ambient temperature and pressure was drawn through the bottom of the aerosol column, through a horizontal 4-in. circular duct, then, flowing upward through the column, the air exited at the top, passing through an absolute filter and being exhausted to the atmosphere by a centrifugal fan. The fan outlet was throttled to produce a flow rate of 1.1 m^3/min through the column. The airflow rate was selected to produce an average vertical velocity of 3.75 m/min within this column. This velocity is a factor of approximately 30 greater than the terminal gravitational settling velocity for water spheres with diameters of 5μm. At the airflow rate selected, it takes approximately 1.6 minutes for one

(a) MARK IX LIDAR VAN

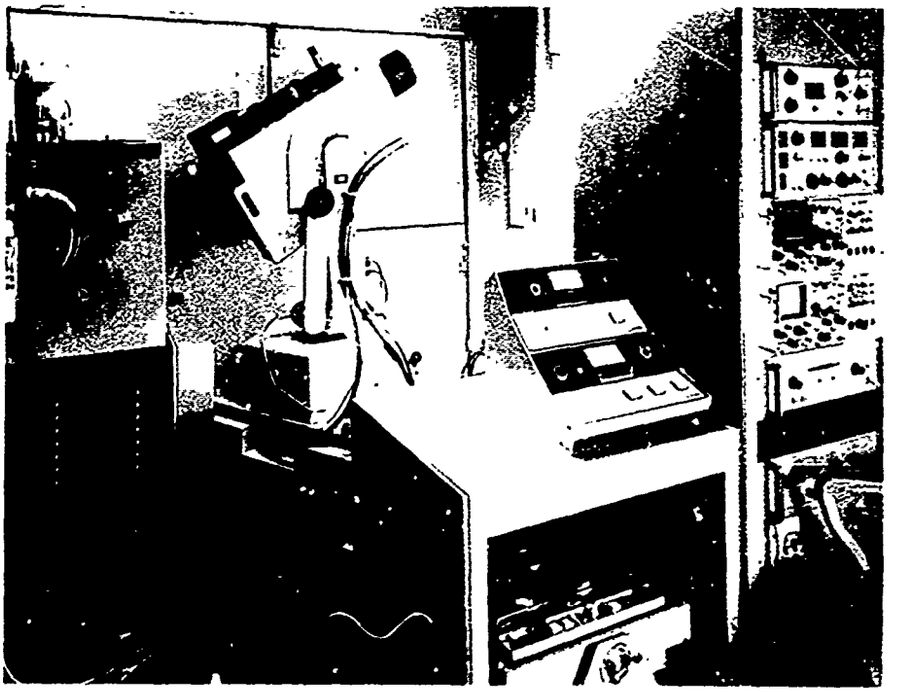

(b) MARK IX LIDAR AND ASSOCIATED RECORDING AND DISPLAY ELECTRONICS

SA-1976-1

Figure 19 The SRI Mark IX lidar system

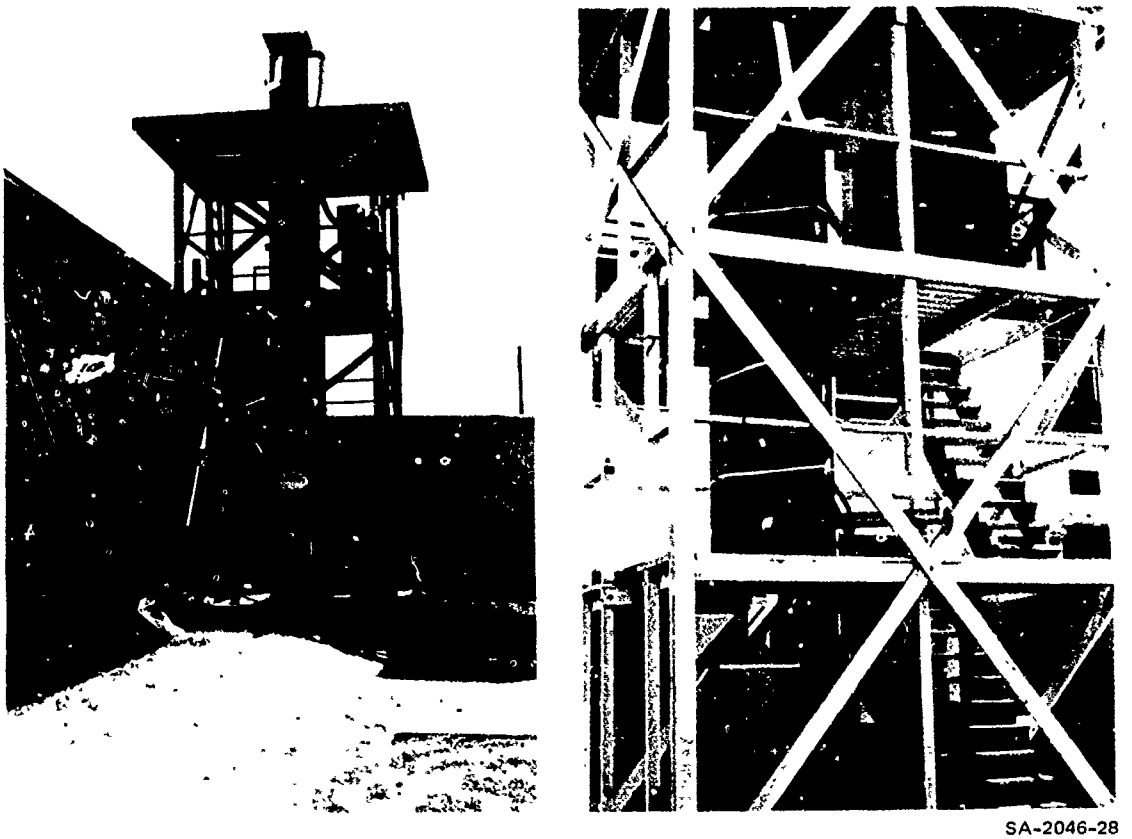

Figure 20 Aerosol column

complete change of air within the column. The airflow rate is measured by a flowmeter, consisting of a manometer (using xylene as the working fluid) to measure the differential pressure across a circular aperture located at the inlet of the 4-in. diameter horizontal duct.

A DeVilbiss Model 35 ultrasonic nebulizer was used to produce the aerosol for the column experiments. This is the same unit used earlier during the laboratory measurement phase of this program (see Section III-b3). The same unit was used to eliminate any potential differences in the physical characteristics of the aerosol, since significant variation in nebulizer performance from one unit to the next could result in changes in size distribution and concentration. For example, variations in the

operating frequency of the ultrasonic transducer would affect the particle size distribution, and variations in the transducer input energy would cause variations in the nebulization rate and therefore in the aerosol mass concentration.

The aerosol was transported from the nebulizer to the inlet duct through a 2-cm diam plastic tube. Turbulent mixing of the concentrated aerosol took place in the horizontal duct, before entering the vertical column.

The approximate concentration of the aerosol was monitored by visual observation of the forward scatter produced by a collimated beam of white light projected horizontally across the column approximately 6 ft above its base. Viewing ports were installed at several locations in the column for this purpose.

D. Remote Sensing Apparatus

The SRI Mark IX lidar was used as the basic remote sensing instrument for these experiments. Several modifications were required to allow the reception of fluorescent returns as well as Mie scattered returns. The details of the Mark IX lidar construction and operation have been extensively described in the literature[11] and will not be repeated here. This section describes the necessary modifications and the operation of the modified instrument.

The output of the Mark IX ruby lidar (wavelength: 6943 Å) was converted to UV radiation (3471.5 Å) by means of a second harmonic generator, using an angle-tuned potassium dihydrogen phosphate (KDP) crystal. The conversion efficiency of this crystal was 2%, yielding approximately 20 millijoules of UV energy. In addition to the UV wavelength, a considerable amount of the primary ruby energy (approximately 700 millijoules) passes unshifted through the second harmonic generator and out

the lidar transmitting optics. Pertinent characteristics of the lidar are listed in Table 5.

Optical beam splitters and dual detectors were added to the receiving optics, in order to receive return signals at both ruby wavelength and at either UV or fluorescent wavelengths. The receiver optical path with the greater transmission losses was selected for the Mie scattering sensor (i.e., this receiver channel is sensitive only to the elastic scattered energy at 6943 Å). The data obtained from this channel were used to monitor the relative density of the aerosol within the column. The receiver optical path with lower transmission losses was used to detect fluorescent radiation from the aerosol cloud. With the appropriate change of wavelength selection filters, this same receiver channel was used to monitor the Mie scattering at the UV wavelength (3471.5 Å).

The maximum detection calculations based on laboratory measurements (Section III) were derived for an optimum laser excitation wavelength. The optimum wavelength could not be used in our field experiments because it was not possible to produce the required wavelengths with existing solid state laser equipment available at SRI. Instead, an organism (P. aeruginosa) was selected whose excitation spectrum was a reasonable (but not optimum) match to the second harmonic of ruby (3472 Å). This arrangement permitted the use of the existing SRI Mark IX lidar system with only the addition of a second harmonic generator to the basic equipment.

Although the laser excitation wavelength did not coincide exactly with the peak of the excitation spectrum of the organism, the laser wavelength did overlap the excitation spectrum enough to allow successful completion of the remote experiments. A check of the data illustrated in Figures 12 and 13 indicated that with the excitation wavelength at 347.2 nm, only about one-half as much fluorescent response was obtained (at 475 nm) from the P. aeruginosa aerosol than would have been obtained with the excitation wavelength at 400 nm.

Table 5: MODIFIED MARK IX LIDAR CHARACTERISTICS

Transmitter	
Laser	Water cooled ruby
Primary wavelength	6943 Å
Second harmonic wavelength	3471.5 Å
Output energy	1 joule/pulse (at 6943 Å)
Pulse width	30 nsec
Q-switch	Pockels cell
Second harmonic generator	KDP
Conversion efficiency	2%
Beam width	0.8 milliradian
Optics	4 x Galilean beam expander coaxial with receiver optics
Pulse rate	60 pulses/min maximum
Receiver	
Optics	15 cm Newtonian reflector
Field-of-view	1 milliradian
Predetection filter passbands	
(a) Primary	10 Å centered at 6943 Å, 0.4 T
(b) Second harmonic	16 Å centered at 3471.5 Å, 0.3 T
(c) Fluorescein	560 Å centered at 5250 Å, 0.29 T
(d) P. Aeruginosa	380 Å centered at 4850 Å, 0.08 T
Detectors (2)	Photomultiplier, RCA 7265 (S-20)
Post-detection bandwidth	35 mHz
Signal conditioning	Logarithmic amplification of lidar returns
Data display	Received power versus time
Data recording	Polaroid photographs

In operation, a small portion of the ruby laser output is converted to UV radiation by the second harmonic generator. This energy is transmitted horizontally toward the aerosol column in a beam approximately 5 cm in diameter with a divergence (beamwidth) of 0.5 milliradians. A significant amount of ruby laser energy is transmitted simultaneously with the UV pulse. Both wavelengths interact with the aerosol cloud, resulting in scattered and reradiated energy at three distinct wavelengths:

(1) Elastic scattering from the aerosol cloud particles at the fundamental laser wavelength.

(2) Elastic scattering from the same cloud particles at the UV wavelength.

(3) Absorption of a portion of the UV energy by the aerosol particles, and reradiation of this absorbed energy over a wavelength interval characteristic of the absorbing material.

The dual-channel optical receiver discriminates between the three returns on the basis of wavelength in the following way: A narrow band interference filter in the ruby channel passes only the fundamental wavelength, and rejects all others. Similarly, the wavelength response of the filter in the fluorescence channel is matched to the spectral characteristics of the fluorescence emission spectrum of the specific target material under study. In addition to passing the desired fluorescence emission spectrum with minimum loss, this filter must also effectively reject Mie scattered energy at both the fundamental and UV wavelengths. This filter must also reject broadband white light produced by the laser pump flashlamp.

E. Experimental Procedure

Two series of remote detection experiments were performed, using a solution of fluorescein and a P. aeruginosa suspension as the aerosol targets. The objective of the first series of experiments was to demonstrate the feasibility of remote detection and to obtain experimental data

to verify the theoretical performance estimate based on laboratory measurements. The objective of the second series of experiments was to demonstrate feasibility, using a more representative target material.

In the first series of experiments, 5% by weight of disodium fluorescein was dissolved in ethylene glycol and further diluted 4:1 with distilled water, resulting in a 1% solution of fluorescein. The purpose of the ethylene glycol was to prevent complete evaporation of the liquid medium during its residence time within the column. The additional dilution with distilled water significantly improved the nebulization characteristics of the solution.

The measured nebulization rate of this solution was 0.3 g/min at a temperature of 20°C with the standard settings on the ultrasonic nebulizer. An airflow rate into the column of 1.09 m^3/min resulted in a calculated aerosol mass concentration of 54 milligrams per cubic meter (mg/m^3) after evaporation of the water, and a fluorescein concentration of 2.8 mg/m^3. The above calculations are based on a particle diameter of 5 μm and a particle number density of 4.2×10^6 per liter (1).

The procedure during the first series of experiments consisted of the following: The closed column was operated for approximately ten minutes with the aerosol generator off, to reach an ambient aerosol concentration within the column identical to the outside atmosphere. Visual and lidar observations verified that the column was clear. The aerosol generator was turned on, set to a predetermined power level, and the aerosol concentration was allowed to build within the column. A minimum of eight minutes was allowed for the concentration within the column to reach a

steady-state condition. Then the upper and lower sliding doors were quickly opened and the lidar immediately fired.*

Typically, two lidar shots were taken within this eight to ten second period. The sliding doors were then closed and the aerosol concentration allowed to again reach a steady-state condition.

This procedure was repeated a number of times to determine variability of signal returns from one shot to the next.

The following experiment was conducted to verify that the fluorescent return was not the result of undesired leakage of laser light into the fluorescence channel of the receiver at either the fundamental or second harmonic wavelength.

A 10% weight solution of sodium chloride in distilled water was nebulized to produce a salt particle aerosol with a concentration of approximately 55 mg/m^3. This nonfluorescing aerosol would have, in general terms, approximately the same reflectivity (i.e., Mie scattering properties) as the fluorescent aerosol. Accordingly, the return in the ruby channel of the modified lidar should be the same for both fluorescent and nonfluorescent aerosols, showing that the same aerosol concentration was present within the column for both series of experiments. However, any return in the fluorescence channel produced by the nonfluorescent aerosol would indicate that reflected energy at the transmitted wavelengths (i.e., 3471.5 Å, 6943 Å) was not being sufficiently attenuated by the matched fluorescence filter.

---

*Although the aerosol within the column could be displaced by air currents when the sliding doors were opened it was shown experimentally that under the near-calm condition that usually prevailed after sunset, the aerosol concentration remained essentially unchanged for at least eight to ten seconds after the doors opened.

The results of this experiment indicated that no observable return was produced by the salt aerosol in the fluorescence channel of the receiver. Thus, the fluorescent return observed in the previous experiment was indeed genuine.

For the second series of experiments, a suspension of P. aeruginosa was prepared, using the procedure described earlier. The cells were allowed to stand at room temperature for four hours* after preparation; 20% ethylene glycol was then added to prevent dehydration of the cells during their residence time within the column. This solution was nebulized and introduced into the aerosol column, following the technique described above.

We considered the possibility that the cell concentration within the aerosol may not necessarily be identical to the concentration of cells within the saline-glycol solution. Preferential nebulization of the saline could reduce the concentration of cells in the aerosol. In any case, we determined the number of viable bacteria in the aerosol column, to be sure that the bacteria were being nebulized.

F. Results

Fluorescence returns were obtained from both aerosols, using the same experimental procedure described earlier. Typical data selected from these experiments are shown in Figures 21, 22, and 23.

Figure 21a shows the lidar return from the region in and around an "empty" aerosol column, that is, the column contains an aerosol representative of the ambient atmosphere. The upper trace shows the output of the fundamental Mie scattering channel (i.e., both transmitted and received wavelengths at 6943 Å). The lower trace in this instance shows the second

*Freshly prepared P. aeruginosa cells exhibit a gradual increase in fluorescence intensity with time. This effect levels off after approximately four hours.

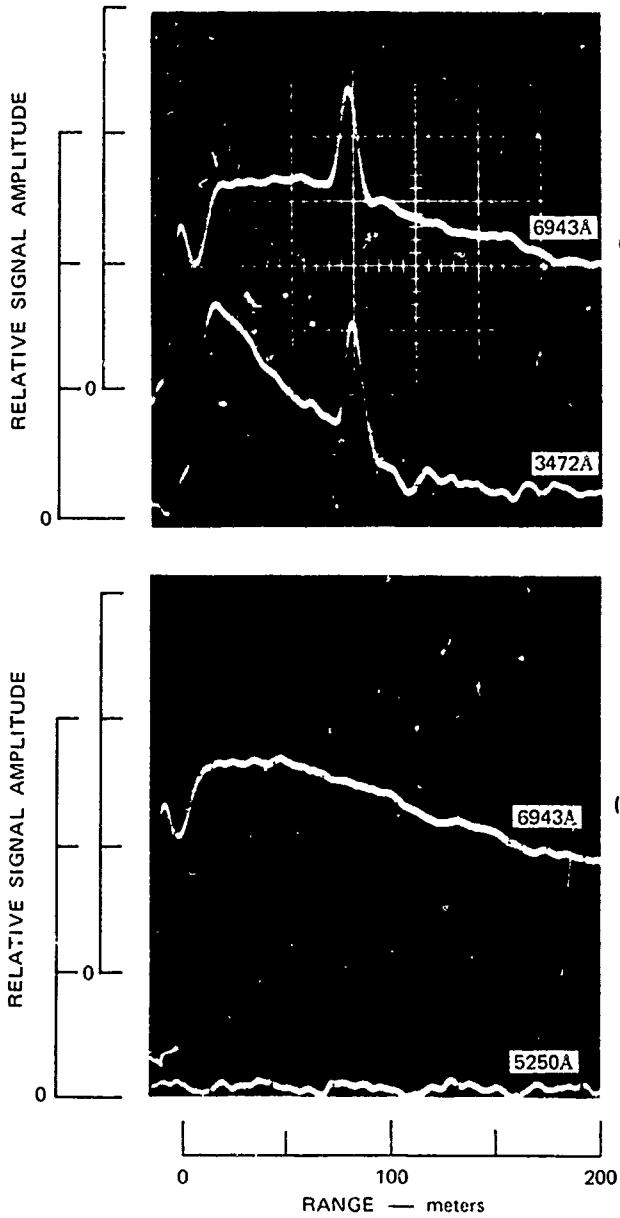

(a) RETURN FROM AEROSOL COLUMN: AMBIENT

Atmospheric concentration.

(b) RETURN FROM AMBIENT ATMOSPHERE ADJACENT TO AEROSOL COLUMN

(Elevation Angle: 10°)

SA-2046-29

Figure 21 Typical examples of remote fluorescence data: fluoroescein aerosol
(Time scale: 200 nsec/div; vertical scale: logarithmic, one decade per two divisions)

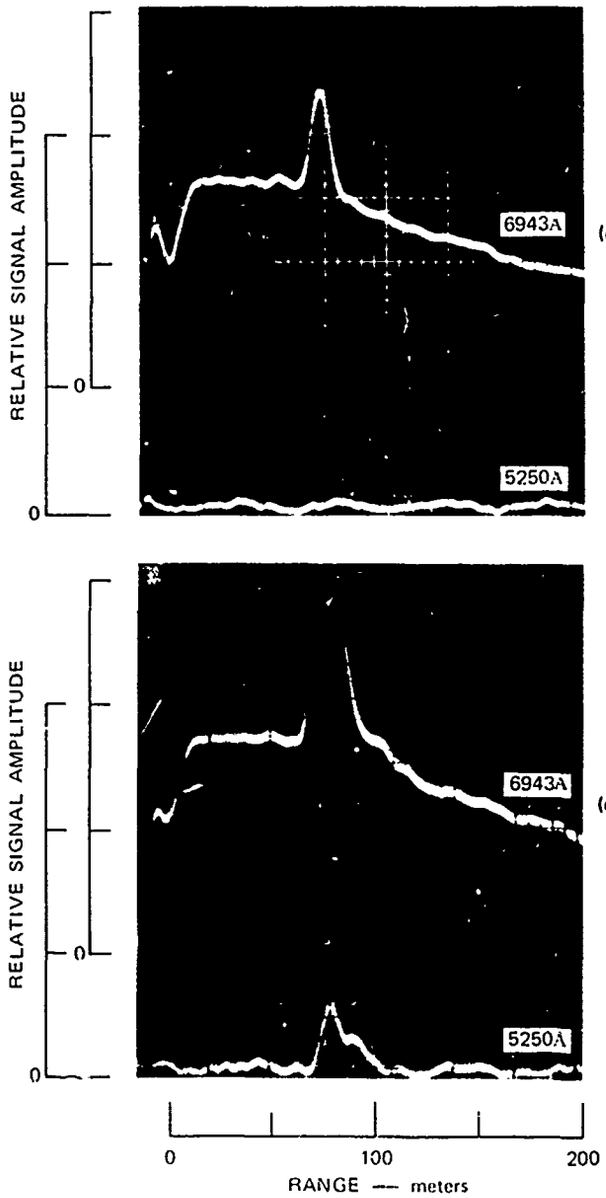

Figure 21 Typical examples of remote fluorescence data: fluoroescein aerosol (Time scale 200 nsec/div, vertical scale logarithmic, one decade per two divisions) (Continuec)

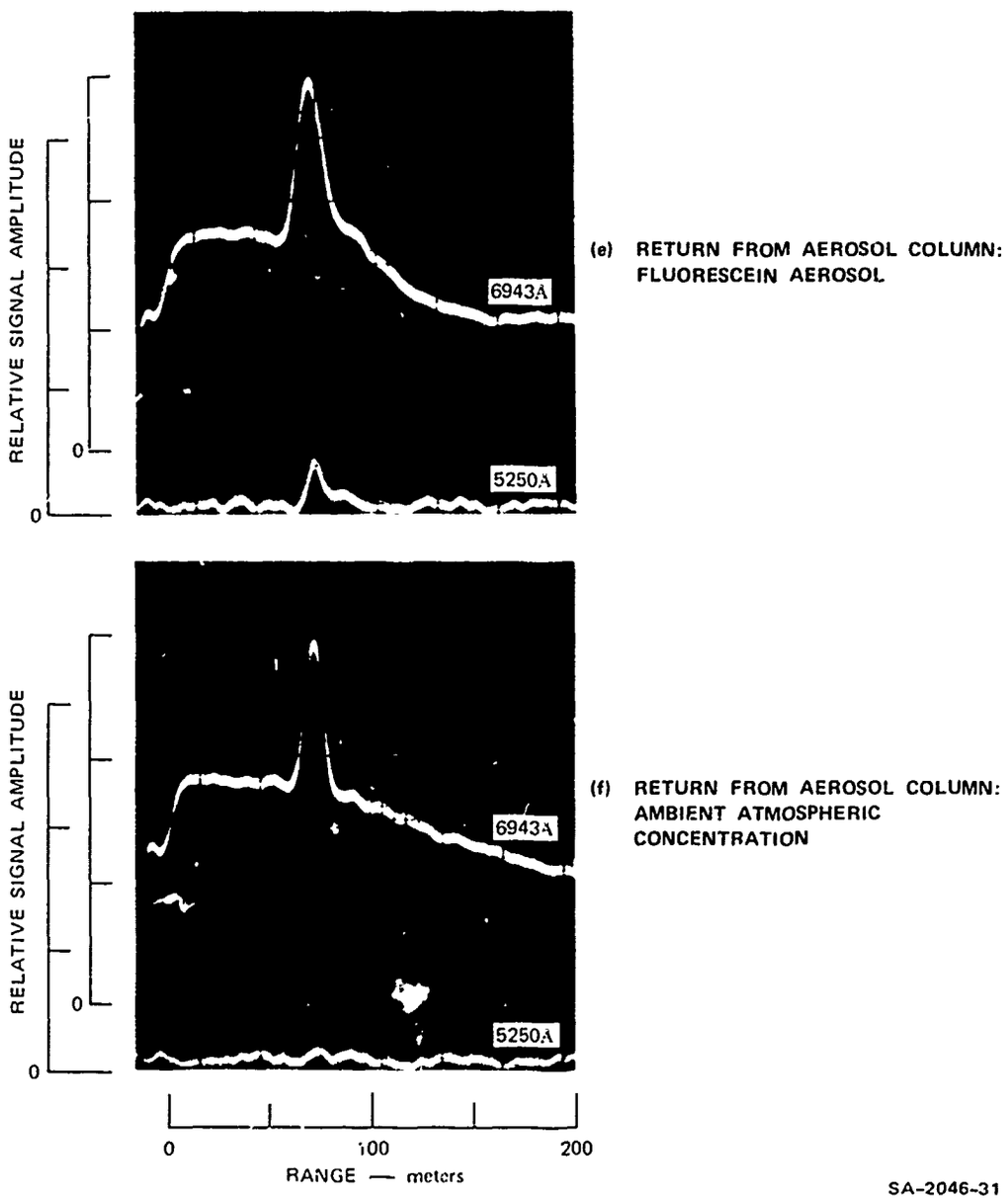

Figure 21 Typical examples of remote fluorescence data: fluoroescein aerosol (Time scale: 200 nsec/div, vertical scale: logarithmic, one decade per two divisions) (Continued)

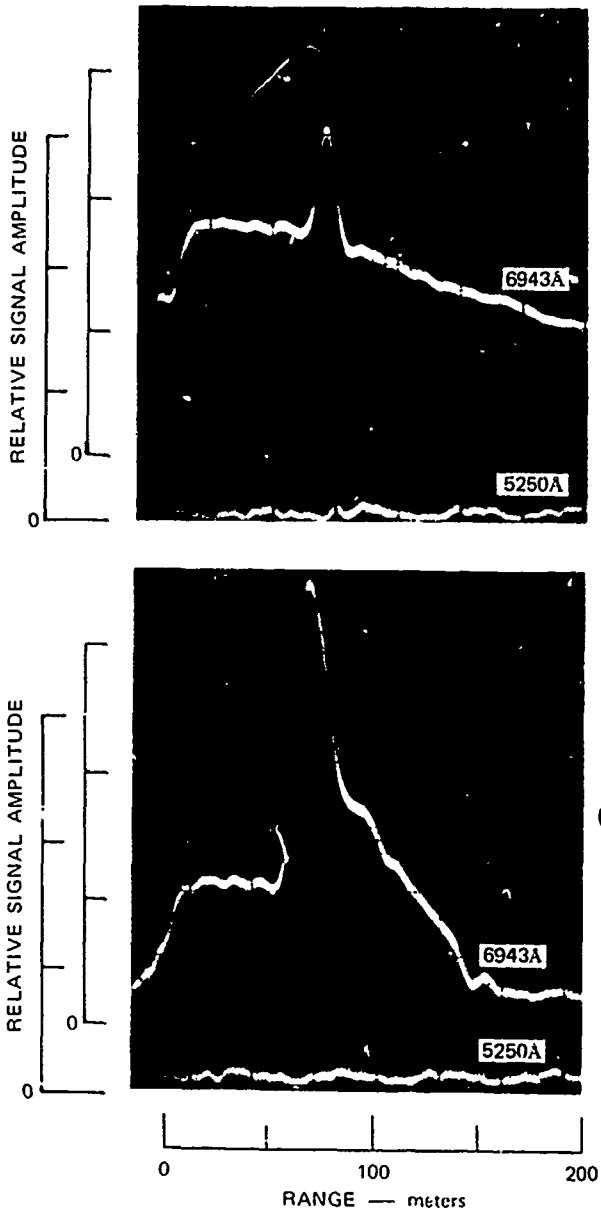

(g) RETURN FROM AEROSOL COLUMN: AMBIENT ATMOSPHERIC CONCENTRATION

(h) RETURN FROM AEROSOL COLUMN: NONFLUORESCING AEROSOL

SA-2046-32

Figure 21 Typical examples of remote fluorescence data: fluoroescein aerosol (Time scale: 200 nsec/div; vertical scale: logarithmic, one decade per two divisions) (Concluded)

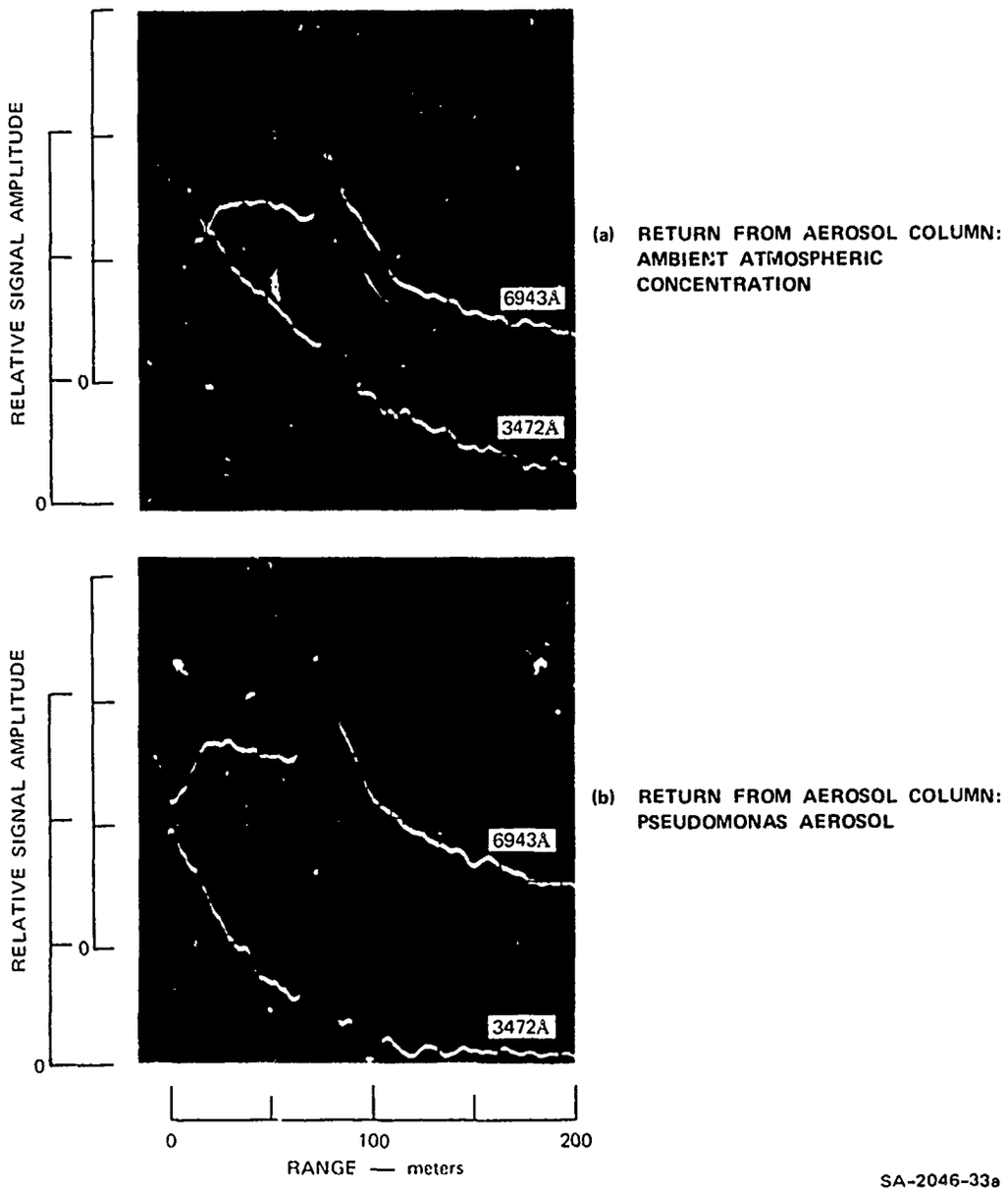

Figure 22 Typical examples of remote fluorescence data: P. aeruginosa aerosol—first experiment (Time scale: 200 nsec/div; vertical scale: logarithmic, one decade per two divisions)

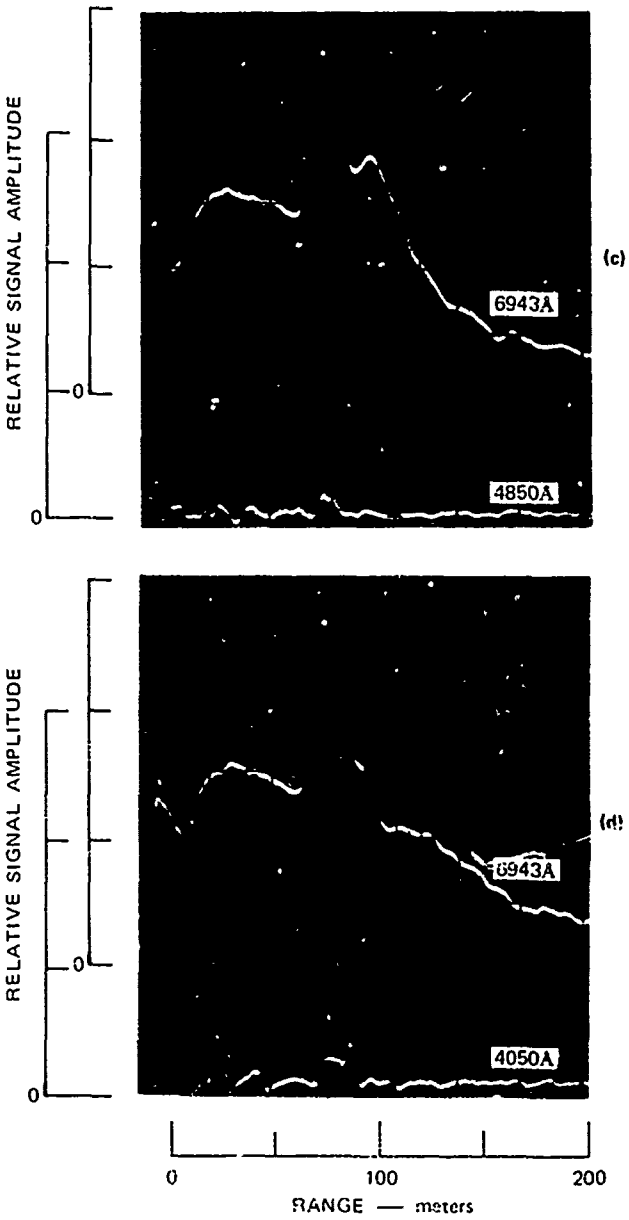

(c) RETURN FROM AEROSOL COLUMN: PSEUDOMONAS AEROSOL

(d) RETURN FROM AEROSOL COLUMN: PSEUDOMONAS AEROSOL

5A-2016-33b

Figure 22 Typical examples of remote fluorescence data: P. aeruginosa aerosol—first experiment (Time scale: 200 nsec/div, vertical scale: logarithmic, one decade per two divisions) (Continued)

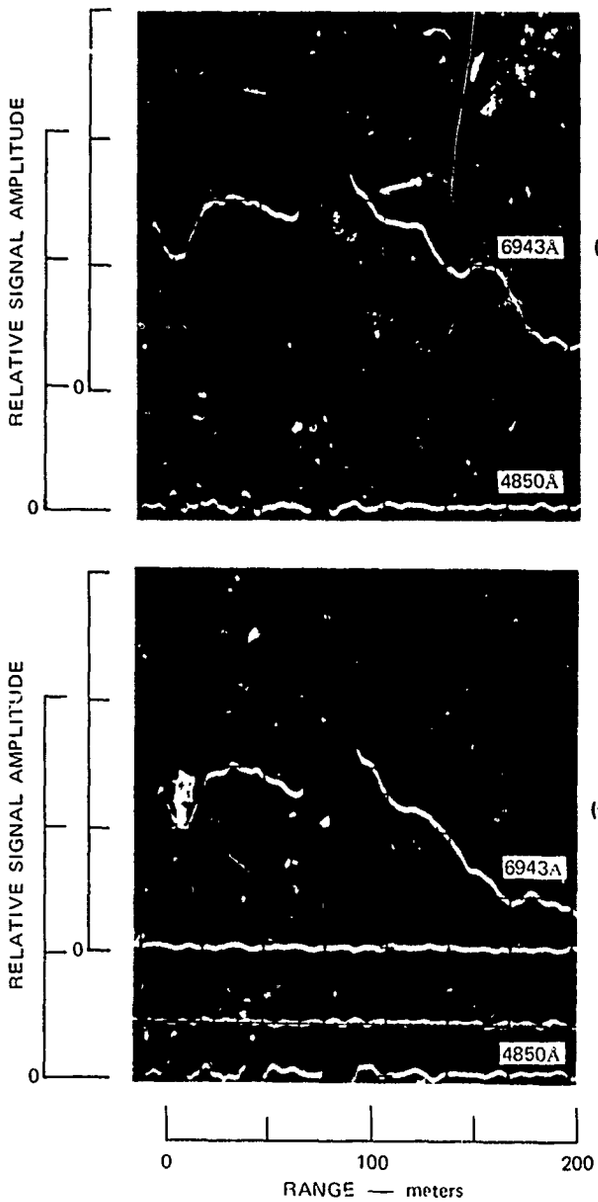

Figure 22 Typical examples of remote fluorescence data: P. aeruginosa aerosol—first experiment (Time scale: 200 nsec/div; vertical scale: logarithmic, one decade per two divisions) (Continued)

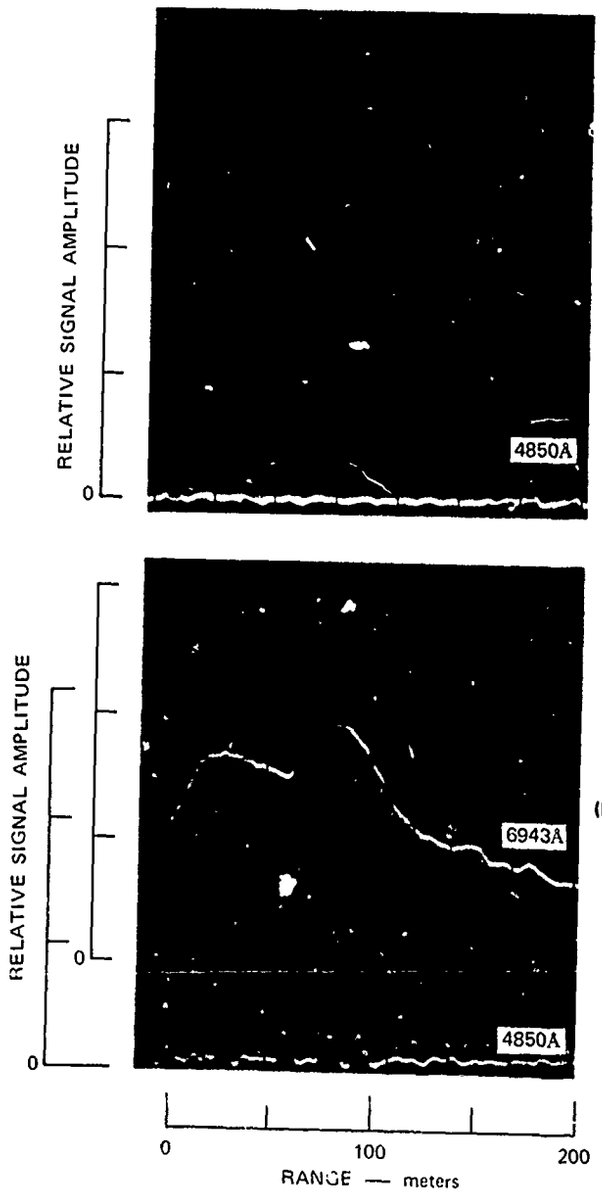

Figure 22 Typical examples of remote fluorescence data: P. aeruginosa aerosol—first experiment (Time scale: 200 nsec/div, vertical scale: logarithmic, one decade per two divisions) (Continued)

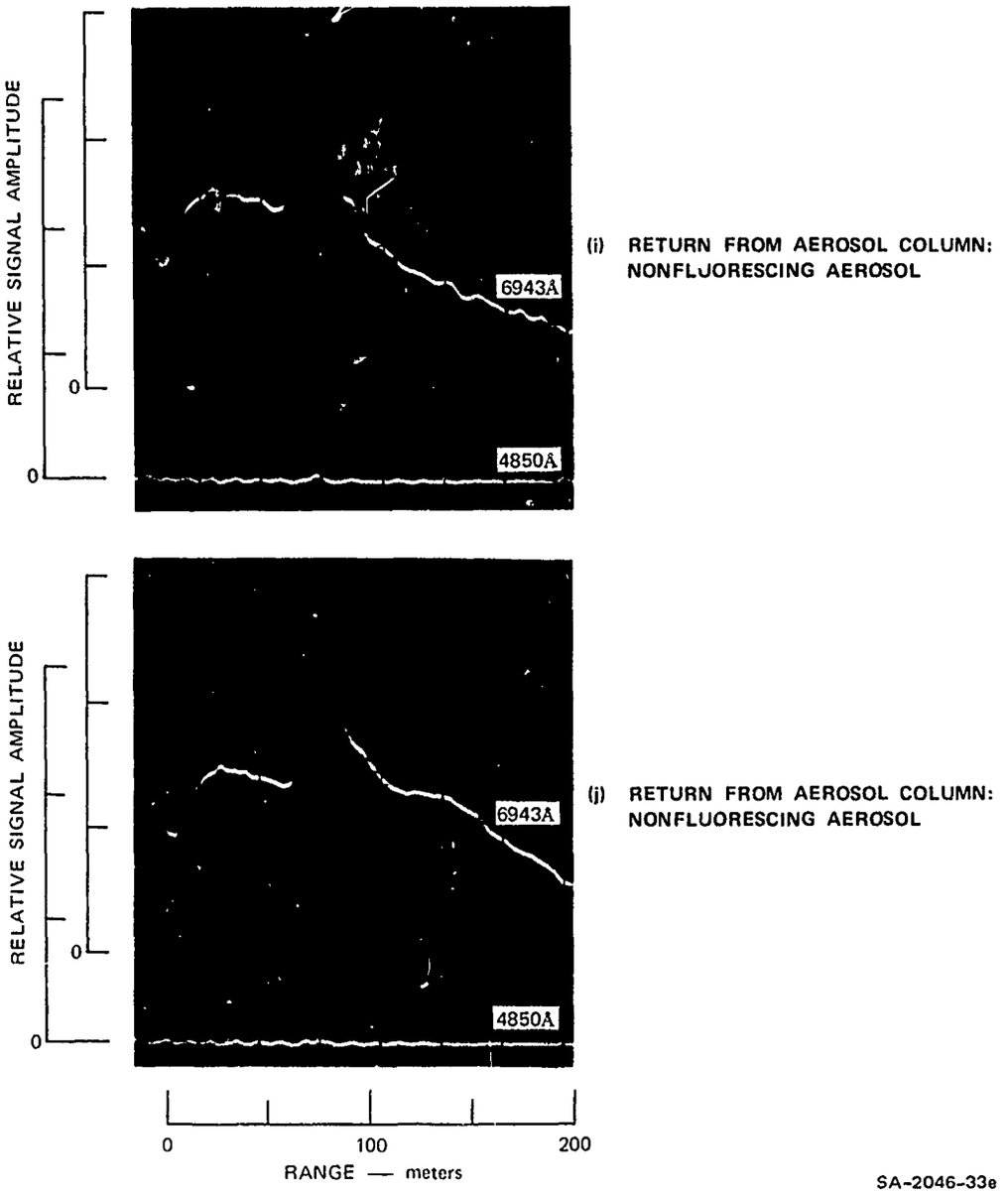

Figure 22 Typical examples of remote fluorescence data: P. aeruginosa aerosol—first experiment (Time scale: 200 nsec/div; vertical scale: logarithmic, one decade per two divisions) (Continued)

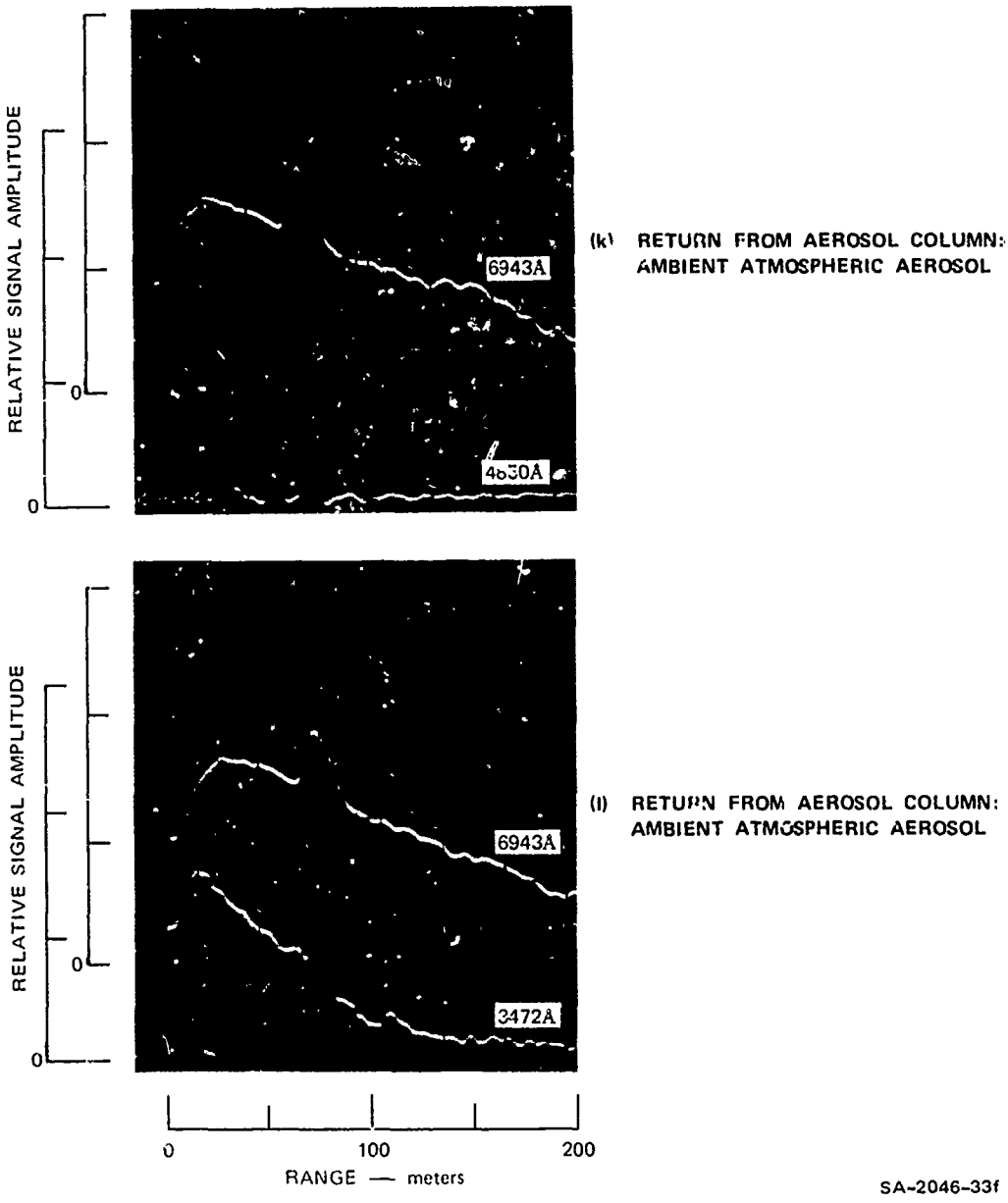

Figure 22 Typical examples of remote fluorescence data: P. aeruginosa aerosol—first experiment (Time scale. 200 nsec/div, vertical scale. logarithmic, one decade per two divisions) (Concluded)

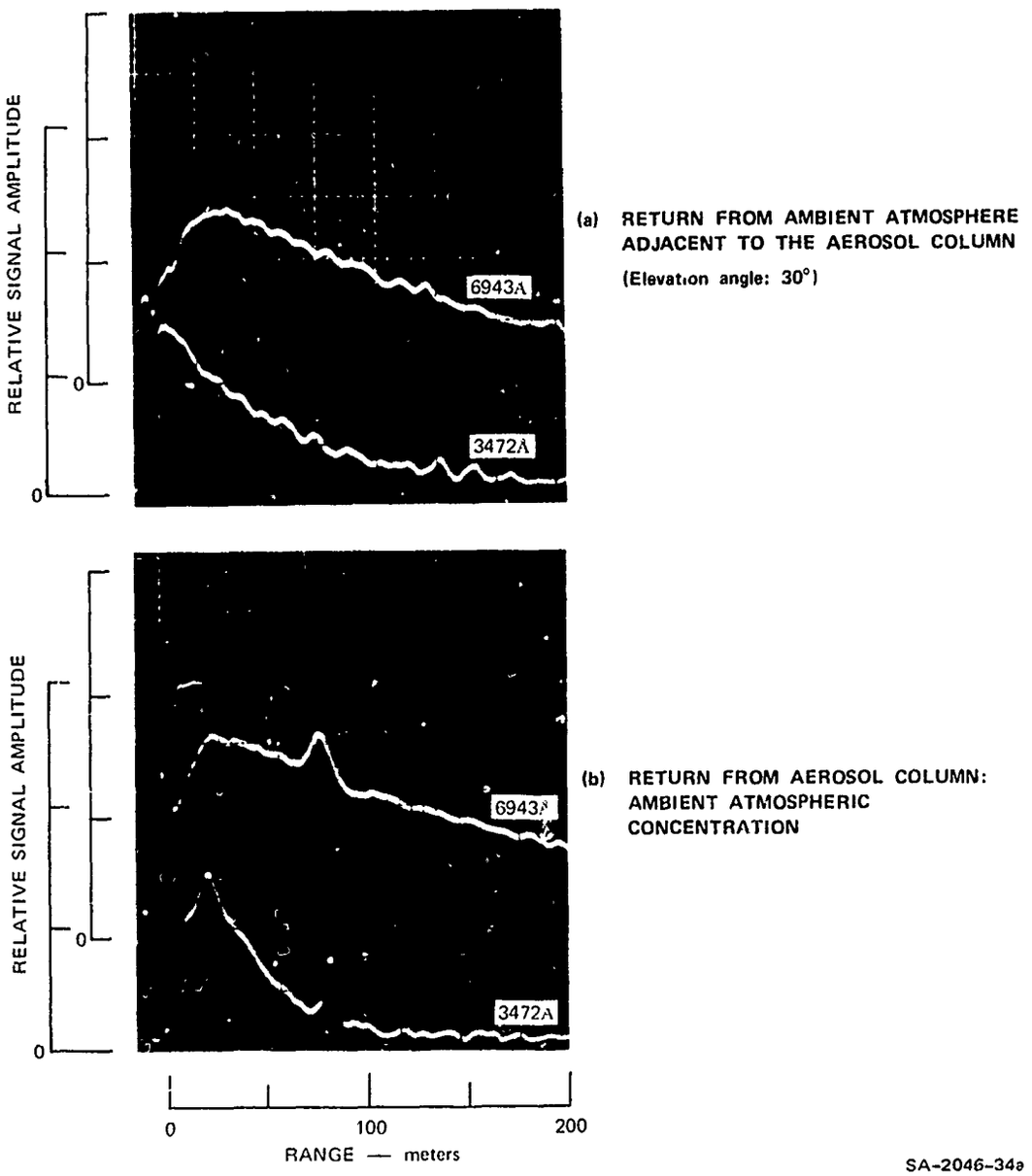

Figure 23 Typical examples of remote fluorescence data: P. aeruginosa aerosol—second experiment (Time scale: 200 nsec/div; horizontal scale: logarithmic, one decade per two divisions)

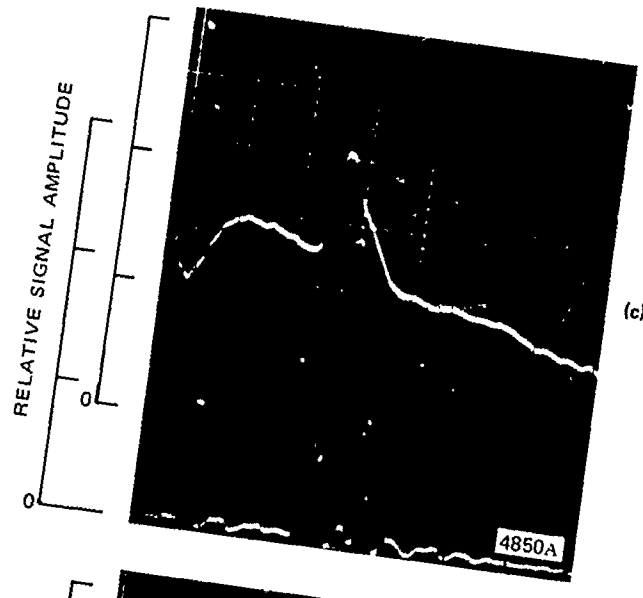

(c) RETURN FROM AEROSOL COLUMN: PSEUDOMONAS AEROSOL

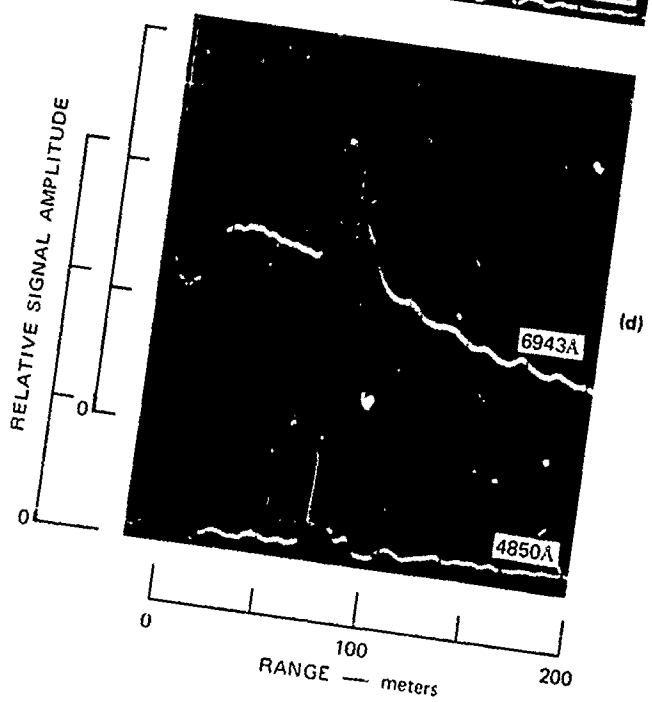

(d) RETURN FROM AEROSOL COLUMN: PSEUDOMONAS AEROSOL

Figure 23 Typical examples of remote fluorescence data: P. aeruginosa aerosol—second experiment (Time scale. 200 nsec/div, horizontal scale: logarithmic, one decade per two divisions) (Continued)

SA-2046-34b

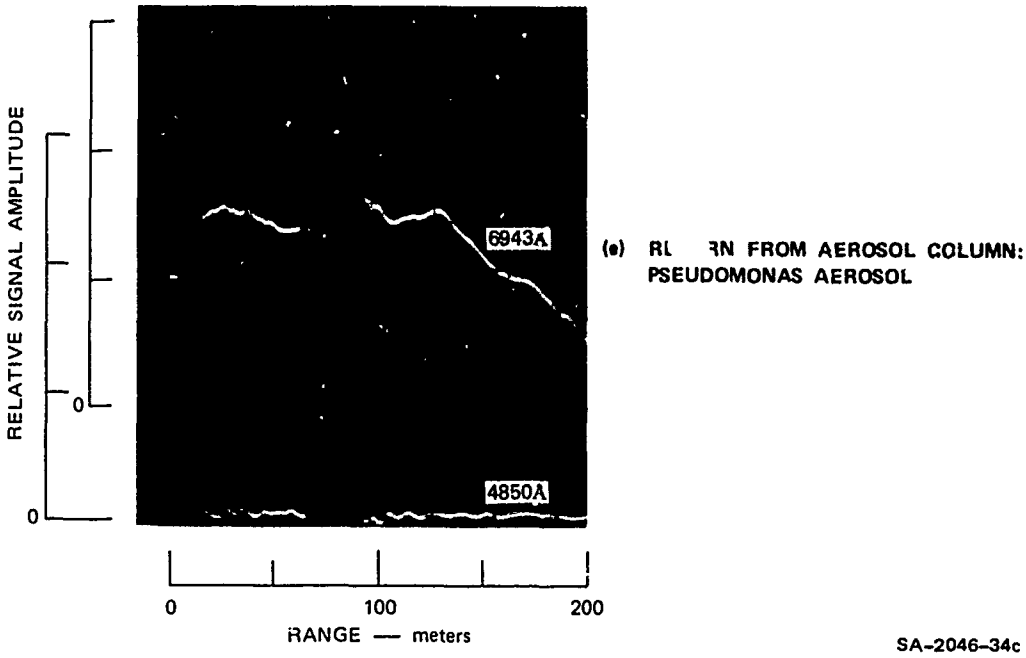

Figure 23 Typical examples of remote fluorescence data: P. aeruginosa aerosol—second experiment (Time scale: 200 nsec/div; horizontal scale: logarithmic, one decade per two divisions) (Concluded)

harmonic Mie scattering return at 3471.5 Å. The peak, located at approximately the 85-meter-range on both traces, is caused by the diffuse reflection from the 45° mirror at the base of the aerosol column. Since the height of the column is only a little greater than the lidar pulse length in space, a lidar return from a dense aerosol within the column would be indicated by an increase in the height of this mirror pulse, together with a slight increase in pulse width. The vertical axes of the figure (received power) are logarithmic and cover three decades of signal intensity from the receiver noise level to maximum signal level. All the lidar data of Figures 21, 22, and 23 conform to this general format, except that the lower trace displays either the fluorescent return or the second harmonic Mie scattering return. The wavelengths associated with each received signal are indicated immediately to the right of the trace.

Figure 21b shows the atmospheric aerosol return on the upper trace. The lower trace shows the absence of any fluorescent return from the ambient atmosphere at fluorescein wavelengths. Note that the mirror pulse is absent in the upper trace because the lidar is positioned off the aerosol column at approximately a 10° elevation angle.

The fundamental and fluorescent returns from the "clear" column are shown in Figure 21c. The mirror pulse is missing in the lower trace because of the absence of any fluorescent materials in the optical path.

The beam-turning mirror located at the base of the aerosol column produced some scattering of both ruby and second harmonic transmitted energy. This scattered energy was detected by both ruby and UV receiver channels (see Figure 22a). The aerosol Mie-scattered return produced within the vertical column appears to coincide with the mirror return because of the close proximity of the mirrors to the aerosol target (less than 0.5 meter) and the finite range resolution of the optical receiver, which is determined by the bandwidth of the logarithmic amplifier (35 mHz).

The presence of the mirror reflection in the ruby or UV receiver chamber was not a severe handicap, because the elastic-scattered return from the aerosol was superimposed on the mirror return. Thus, the aerosol concentration within the column could be monitored by means of elastic-scattering return from the ruby receiver channel, as long as the scattering produced by the turning mirror remained constant. Dust deposits on the surface of the mirror could produce a higher amplitude mirror return in both ruby and UV receiver channels. However, careful cleaning of the mirror between aerosol runs minimized this effect. Also, the mirror return was verified by monitoring the mirror return amplitude with an "empty" aerosol column (Figure 22e) after each experiment.

The mirror return was <u>not</u> present in the signal obtained from the fluorescent receiver channel (Figure 22k), for two reasons:

- The fluorescent channel predetection filter blockage for both fundamental and second haromonic wavelengths was sufficient to suppress any transmitted energy leakage at these wavelengths.
- The evaporated aluminum front-surface mirror does not exhibit any fluorescence effects.

The Mie scattering return and fluorescent return from a fluorescein aerosol is shown in Figure 21d. The aerosol mass concentration is greater than the ambient aerosol by a factor of approximately five, as indicated by the increase in height of the return from the mirror and aerosol column in the upper trace. The fluorescent return is shown in the lower trace. The same experiment is repeated in Figure 21e. Figure 21f shows the return from a "clear" column. Note that the mirror return in this case is of greater amplitude than in Figure 21c, because a small fraction of the aerosol from the previous experiments had settled onto it. When the mirror is cleaned, the mirror return is comparable to that of Figure 21c.

The optical returns from a nonfluorescent aerosol are shown in Figure 21h. The mass concentration of this aerosol is greater than the ambient atmosphere by approximately a factor of 40. The fundamental Mie scattering receiver in this experiment was desensitized by a factor of 10. The lack of a fluorescent return on the lower trace indicates an adequate degree of blockage of both fundamental and second harmonic transmitted wavelengths.

The wave forms in Figure 22 were obtained from the first experiment with P. aeruginosa. The format, content, and experimental method are identical with those discussed for the previous figure. Figure 22a shows a return from a background aerosol column at both fundamental and second harmonic wavelengths. Figure 22b shows fundamental and second harmonic wavelengths from P. aeruginosa aerosol. Figures 22c, 22d, 22e, and 22f show the Mie scattering return and the fluorescence return from this aerosol. The additional pulse returns on the lower traces of Figures 21d,

21e, and 21f, which occur at ranges between 0 and 50 meters, are caused by electrical interference from the laser flashlamp. The two additional horizontal lines in Figure 22f were produced by inadvertent triggering of the oscilloscope and have no significance. Figure 22g shows a typical example of these interfering pulses, obtained by occluding the transmitter aperture. They appeared at random positions along the horizontal axis at intermittent intervals during the course of this series of experiments. Figures 22h, 22i, and 22j illustrate the returns from a nonfluorescing aerosol. The lack of a fluorescent return on the lower trace indicates adequate optical blockage of the transmitted exciting wavelengths from the receiver. Figures 22k and 22ℓ show the returns from an ambient atmospheric aerosol. The returns in the lower trace of Figure 22k are produced by electrical interference noted before, further evidenced by a lack of spatial correlation in the upper and lower traces.

Data obtained from the second experiment with P. aeruginosa are shown in Figure 23. The fluorescent returns are shown in Figures 23c, 23d, and 23e. The direct sampling of aerosol within the column, mentioned previously, was done during this experiment.

The remaining sequences in this experiment could not be completed because the detector in the fluorescence channel was inadvertently saturated during the course of the experiment. From previous experience, saturation of this kind results in a temporary degradation in sensitivity of between one and two orders of magnitude, so it was considered pointless to continue the experiment at this time.

The signal/noise (S/N) ratio applicable to the pseudomonous experiments in the outdoor chamber is on the order of 5 decibels (dB), based upon the amplitude of the fluorescence return signals of Figures 23c, 23d, and 23e, and the noise level of the fluorescence receiver channel of Figure 22g. That is, the peak value of the fluorescence return signal is at

least 5 dB above RMS receiver noise level. In these experiments, the receiver noise level was comparatively low for two reasons: first, since the experiments were conducted at night, the amount of ambient light scattered into the fluorescence receiver channel was very low, in spite of the relatively wide spectral bandwidth of the optical predetection filter employed. Second, the photomultiplier detector was operated at a relatively low gain (anode voltage of 1.3 to 1.9 kilovolts) corresponding to a photomultiplier gain of 10^5, compared to the maximum gain of 10^7 for this detector.

In summary, fluorescent returns were received from both the fluorescein and microorganism at a distance of 90 meters, under simulated field conditions. In neither series of experiments was there any evidence of leakage of laser excitation energy into the fluorescence channel of the receiver. Also, the fluorescence background returns from the ambient atmospheric aerosol were not observed during these experiments.

During the last experiment of this second series, a slit sampler and an all-glass impinger[12] (both instruments provided by the sponsor) were used to collect aerosol samples from several locations along the height of the aerosol column. The sampling was done immediately before and after the lidar observations.

Two samples were taken with a one-minute slit sampler adjusted to a flow rate of 14.2 l/min. Particles were collected on agar plates and, after incubation, the number of colony forming units (cfu) were counted. We estimate 3 cfu/mm^2 and 10-12 $\times$ 10^3 mm^2/plate. Area estimates were made by cutting out a paper template and weighing it. The airflow rate through the instrument was 14.2 l/min, and 3 $\times$ 10^4 - 3.6 $\times$ 10^4 cfu were collected. We therefore estimate that there were approximately 2.1 to 2.5 cfu/ml of air within the column.

Samples were also taken with an all-glass impinger. The bacteria were collected in 20 ml of saline and then plated out to determine the number of cfu. Two 1-ml samples were taken at a flow rate of 12.5 liters of air/min. In the first run, a 0.1 sample of a 1:10 dilution gave an average (3 plates) of 56 cfu/plate. In the second run, a 0.1-ml sample of a 1.10 dilution gave an average of 72 cfu/plate. It follows that

$$\text{cfu/ml of air in tunnel} = \frac{(56 + 72) \times 100 \times 20}{25000 \text{ cc}} = 10.2 \qquad (15)$$

where the numerator describes the product of cfu/plate, dilution factor, and saline volume, respectively, and the demoninator describes the volume of air sampled.

G. Discussion and Summary of Results--Phase II

Although the modified Mark IX lidar has successfully demonstrated the feasibility of remote fluorescence detection, the basic design of this equipment does not represent an optimum configuration for the specific use of this project. The Mark IX lidar is intended to be a general purpose research facility which could easily be adopted to a wide variety of experiments. Thus a significant improvement in sensitivity is possible with a sensor optimized for this particular application. The lack of sensor sensitivity is not considered a serious drawback in this early stage of investigation. Once the detection limits of the present experimental equipment are determined (using fairly high aerosol concentrations at close ranges), the performance of other hypothetical systems may be accurately estimated by extrapolation of the experimental data.

The performance differences between the experimental equipment and a state-of-the-art optical sensor may be estimated on the basis of known optical parameters, available laser energy, and detector sensitivities.

Table 6 lists the degree of improvement which could be obtained in progressing from the modified Mark IX lidar used in our experiments to a sensor of optimal design. The total improvement is 55.7 dB, representing a factor of 3.7×10^5 improvement in sensor sensitivity. Returning to the data from the first series of experiments involving fluorescence, the calculated number density of fluorescent particles within the column is 4.2×10^6 per liter. Since the fluorescence emission is a linear function of number density, any improvement in sensor sensitivity translates directly into a decreased number density of particles required to achieve detection. Accordingly, the optimal sensor will be able to detect an aerosol number density of approximately 11 particles per liter at a range of 90 meters. For a given sensor sensitivity, as the range to a target is increased, the minimum detectable aerosol concentration increases as the square of range. Accordingly, when the range is increased from 90 meters to 1 km, the minimum detectable aerosol concentration increases to:

$$11 \left(\frac{1000}{90}\right) 2 = 1358 \text{ particles/liter} \quad .$$

When the range is increased from 90 meters to 2 km, the minimum detectable concentration increases to:

$$11 \left(\frac{2000}{90}\right) 2 = 5432 \text{ particles/liter} \quad .$$

Atmospheric extinction, in general, will result in additional attenuation of the received optical signal over and above the R^{-2} relationship described above. The possible effect of atmospheric extinction was investigated by means of computer-based optical propagation models. It was determined that for the relatively short ranges under consideration here (in the order of 1-2 km), atmospheric extinction has only a slight effect.

Table 6: MODIFIED MARK IX LIDAR-OPTICAL LOSSES

Mark 9 (Modified) Lidar Losses

Transmitter	7.371×10^{-3}	-21.33 dB
Receiver	3.861×10^{-1}	-4.18 dB
Optical filter	2.963×10^{-1}	-5.28 dB
Atmospheric losses	9.55×10^{-1}	-0.20 dB
Total	7.96×10^{-4}	-30.99 dB

Theoretical improvement to obtain lossless performance at 1 J/pulse output at 3471 Å

Eliminate above losses	30.99 dB
Pulse counting	26.99 dB
Quantum efficiency improvement	1.25 dB
12" receiver aperture	6.00 dB
	65.23 dB

Corrections to "lossless" system to allow for practical losses

Optical losses	-5.09 dB
Atmosphere losses	-4.46 dB
Total	-9.55 dB

Net Improvement 55.7 dB (3.7×10^5)

Returning to the second series of experiments involving P. aeruginosa the number density of cells, as measured by the all-glass impinger (AGI), was 10,200 cfu/liter within the column. Extrapolating these data yields the following minimum detectable concentrations at 2 km using an optimal sensor:

$$\frac{1.02 \times 10^4 \text{ cells/l}}{3.7 \times 10^5} \left(\frac{2000}{90}\right)2 = 13.6 \text{ cells/liter} \quad .$$

This estimate assumed that the number of cfu/liter in the column is nearly the same as the number of cells/liter in the column.

These estimates of minimum detectable particle concentration at a given range are based upon a fluorescent receiver channel S/N ratio of 5 dB, identical to the S/N ratio observed in the outdoor experiments. The above estimates are based upon a 12-inch-diameter optical receiver, with low-loss internal optics, operating in the pulse counting mode, and with an improved quantum efficiency photocathode. A laser output energy of 1 joule per pulse, with low-loss transmitter-optics is also assumed. The remaining factors, such as excitation and fluorescent wavelengths and receiver filter bandwidths, are identical to the ones used in the short range outdoor experiments.

In the foregoing calculations, one joule per pulse transmitted energy was assumed. Although this energy output is not routinely available today at UV wavelengths, it appears to be achievable during the next five-year period, taking into consideration the developments in oscillator-amplifier lasers, and in doubled dye lasers.

The software improvement attributed to the pulse-counting mode of detection is made on the basis of previous SRI experience in using this technique for the detection of extremely low optical signals. The 26.99-dB improvement in system sensitivity is based on the use of a photomultiplier detection when it is optimized for photon counting along with state-of-the-art electronic pulse discriminators and counters.

V CONCLUSIONS

The optical properties associated with the fluorescence of microorganisms were investigated by means of laboratory and remote sensing experiments. The excitation and emission spectra of several microorganisms (in liquid suspension and in aerosol form) were obtained in the laboratory by means of a calibrated spectrofluorometer.

Performance calculations of a hypothetical optical sensor were then made, based on data obtained from an analysis of the fluorescent spectra. These calculations indicate that a detection range in the order of 1-2 km could ultimately be achieved at sea-level midlatitude geographical locations. Based on these positive results, remote sensing experiments were initiated.

The remote sensing experiments were performed to demonstrate the basic principle of remote fluorescence detection under simulated field conditions and to extrapolate the performance of this experimental equipment to remote fluorescent sensors specifically designed for this application.

Fluorescent returns were obtained at a range of 90 meters from both fluorescein and P. aeruginosa aerosols under ambient sea-level atmospheric conditions. The SRI Mark IX lidar, modified for fluorescence work, was used as the experimental sensor. Fluorescent background radiation from ambient atmospheric aerosol was not observed during these experiments.

Direct biological sampling of the aerosol within the column was done immediately before and after the lidar observations, by means of a slit sampler and an all-glass impinger (AGI). The number density

of P. aeruginosa aerosol as measured by the AGI was 1.02×10^4 cfu/liter.

The lidar data were normalized for the significant optical losses inherent in this experimental equipment. An extrapolation of the normalized data indicates that a minimum detectable concentration, in the order of 14 cells/liter, could be detected at a range of 2 km by a state-of-the-art optical sensor. Atmospheric attenuation effects appropriate to sea-level conditions at midlatitude geographical locations were considered in these calculations.

In addition, the laboratory experiments have identified several optical interactions which, if unique, could be used to advantage in a remote optical sensor.

Although the fluorescent spectra of microorganisms are typically composed of characteristically broad, featureless bands which are of little diagnostic use, we have found that the excitation spectra are typically sharper and show detailed structure in some of the cases examined. This feature, in principle, could be used to remotely discriminate between specific classes of microorganisms, by tuning in wavelength over the appropriate excitation wavelength intervals. Therefore, when feasible, the remote-sensing application of tunable lasers would be advantageous.

In addition to excitation spectra, which appear to be characteristic, the tryptophan peak appeared in all bacterial spectra obtained to date. Based on limited experimental data, this peak appears to be a distinguishing feature of microorganisms. If the tryptophan peak can be reliably detected in a broad category of organisms, the lidar return at tryptophan wavelengths could serve as a reliable, generalized indicator of bacterial aerososls. This technique would not require the optical sensor to possess a wavelength-scanning capability. Its primary usefulness appears to be

in the detection of a wide range of microorganisms, with an optical sensor operating at the tryptophan wavelength.

The polarization properties of several microorganisms in bulk liquid suspension were examined in the spectrofluorometer. Although most measurements indicated an 80-90% depolarization of the fluorescent radiation, several intriguing effects were noted. For a given microorganism suspension, some excitation bands show total depolarization; other bands for the same organism show a strong polarization with very little rotation; further bands of the same organism show strong polarization with approximately 90° rotation. These experiments suggest that polarization may be another useful diagnostic parameter in remote sensing, but more experimental information is required to fully evaluate its potential usefulness.

The fluorescent lifetimes of several organisms were measured at the peak of their respective excitation and emission bands. These lifetime measurements tend to fall in the 6-10 nsec range, significantly shorter decay times than those of typical Q-switched laser pules. Accordingly, unless specific bands are found that exhibit significantly longer fluorescent lifetimes, the diagnostic potential of this technique seems rather limited.

In addition to monitoring the optical properties of aerosols, which are primarily determined by the chemical and biological considerations, a remote optical sensor can also respond to physical changes of an aerosol cloud. These changes include increases in cloud volume, and translation downwind, as well as changes in the vertical distribution of particle size or function of time. An aerosol diffusion model was used to evaluate the cloud behavior for two specific particle size distributions (mass median diameter of 6 μm and 50 μm). For the smaller size distribution (the one likely to be of most interest), the particles are small and settle very slowly, and there is little difference in

particle size distribution as a function of position within the cloud. The linear shape of an artificial cloud, combined with observable changes in the lidar return over a period of time, could usually distinguish an artificial cloud from a natural one.

The experiments conducted to date suggest that the above optical interactions have potential value as additional diagnostic parameters in remote sensing applications. Specifically, the signal-to-noise ratio or the specificity of an optical sensor may be improved significantly. However, more experimental information is required to properly evaluate the potential usefulness of these techniques.

VI RECOMMENDATIONS

Favorable results at the conclusion of the present phase of the research effort cannot yet form the basis for immediate investment in specialized prototype hardware, because of two major areas of risk, outlined below.

- Estimates of feasibility are currently based on measured fluorescent spectra of a relatively few classes of organisms. These performance estimates may not necessarily be representative of a broader class of organisms, including potentially hazardous ones.
- The magnitude and characteristics of the fluorescence signature associated with various ambient atmospheric conditions (including seasonal and geographic variations) have not yet been investigated.

The above parameters can significantly affect the S/N ratio of any proposed remote sensing system, and thus impose practical limits on the performance of the system.

To reduce the financial and technical risk inherent in the immediate construction of prototype equipment, the following exploratory research plan is proposed. The objective of this suggested course of action is to define in detail the operating parameters of a remote sensing system, and to identify the practical limitations on system performance imposed by:

(1) The physics of the fluorescence process

(2) The limitations imposed by the ambient atmosphere

(3) The limitations imposed by electrooptics technology.

The following tasks are suggested:

Task 1

(1) Investigate a broader class of materials and practical nutrients.

(2) Define the wavelength domain occupied by the excitation and emission spectra of a broad class of materials and practical nutrients.

(3) Determine how well single specific laser wavelengths or multiple wavelengths achievable with a tunable laser can be utilized to detect effectively several classes of organisms.

(4) Obtain excitation and emission spectra of a broad class of practical nutrients to determine the significance of possible masking effects (where the fluorescence signature of the organism is modified or obscured by the fluorescence associated with the accompanying nutrient solution).

Task 2

Investigate the atmospheric background fluorescence problem at appropriate excitation and fluorescence wavelengths. Once the wavelength domain of operation has been defined for both fluorescence excitation and emission, then the magnitude and character of atmospheric background fluorescence processes could be investigated within the wavelength domain of interest, to determine the significance of atmospheric background considerations on system performance.

Task 3

Investigate techniques to improve S/N ratio or specificity. Other optical properties associated with fluorescence, such as fluorescent lifetime and polarization, have been briefly investigated in the present work, because they constitute independent characteristic properties of organisms. Preliminary results indicate that those optical properties may be utilized in one, or both, of two ways: (1) to increase the

specificity of the sensing system, thus rejecting nonviable aerosols and; (2) to increase the S/N ratio of the system, thereby improving its maximum range capability.

The measurements required for this task (such as fluorescent lifetimes and polarization) should be accomplished in conjunction with the measurements in Task 1.

Task 4

Extend the concepts developed during the present work regarding prediction of performance of remote sensing optical systems, based on laboratory measurements of aerosols. The ability to predict this performance accurately will result in significant savings in time and effort, compared with an extensive program of field testing.

Task 5

Investigate the potential of remotely denaturing protein, by means of a carbon dioxide laser, to allow reliable distinction between a viable hydrated culture with organisms and a harmless dry dispersion of organic or inorganic matter. This procedure could significantly reduce the probability of false alarms.

Task 6

Develop a detailed design and cost estimate for a prototype optical system. The information obtained in the tasks outlined above will form the basis for a reliable, detailed evaluation of the practical feasibility of an optical remote sensing system. In particular, it will identify the scope and extent of practical limitations that could influence the design and performance of a prototype. The objective of this task will be to define in detail the optical and electronic design and cost estimate

for the construction of a prototype sensing system which would make maximum use of the current state of the art in electrooptical technology.

The decision to proceed with prototype construction would thus involve a low level of technical risk, and the probability that the prototype would meet its performance objectives would be increased accordingly.

LITERATURE CITED

1. "Aerosolized Microorganism Fluorescence Study," IBM Final Report for Department of the Army, Fort Detrich, Maryland, Contract No. DAA4-13-68-C-0180 (May 1969).

2. H. Kildal and R. L. Byer, Proc. of The IEEE, 59, 1644-1663 (1971).

3. J. Gelbwachs and M. Birnhaum, Applied Optics, 12, 2442 (1973).

4. S. V. Konev, Fluorescence and Phosphorescence of Proteins and Nucleic Acids, Plenum Press, New York (1967).

5. E. Gaviola, Ann. Physik 81, 681 (1926).

6. A. Muller, R. Lumry, and H. Kokubun, Rev. Sci. Instr. 36, 1214 (1965).

7. S. V. Volkov, L. A. Limoreva, and V. I. Shirouv, Bull. Acad. Sci. USSR 27, 555 (1963).

8. S. S. Brody, Rev. Sci. Instr. 28, 1021 (1957).

9 D. H. Slade, "Meteorology and Atomic Energy, USAEC, Division of Technical Information, Report TID24190 (1968).

10. M. Smith, Editor, Recommended Guide for the Prediction of the Dispersion of Airborne Effluents, A.S.M.E. (1968).

11. R. J. Allen and W. E. Evans, "Laser Radar (Lidar) for Mapping Aerosol Structure," Rev. of Sci. Instr., 43, 1422 (1972).

12. U. S. Department of Health, Education, and Welfare, "Sampling Microbiological Aerosols," Public Health Service Monograph No. 60, Washington, D.C. (1959).